BRNO UNIVERSITY OF TECHNOLOGY
VYSOKÉ UČENÍ TECHNICKÉ V BRNĚ

FACULTY OF ELECTRICAL ENGINEERING AND COMMUNICATION
FAKULTA ELEKTROTECHNIKY
A KOMUNIKAČNÍCH TECHNOLOGIÍ

DEPARTMENT OF RADIO ELECTRONICS
ÚSTAV RADIOELEKTRONIKY

NEURAL MODELING OF ELECTROMAGNETIC FIELDS IN CARS
NEURONOVÉ MODELOVÁNÍ ELEKTROMAGNETICKÝCH POLÍ UVNITŘ AUTOMOBILŮ

DOCTORAL THESIS
DISERTAČNÍ PRÁCE

AUTHOR — **Ing. Martin Kotol**
AUTOR PRÁCE

SUPERVISOR — **prof. Dr. Ing. Zbyněk Raida**
ŠKOLITEL

BRNO 2018

ABSTRACT

The dissertation thesis is focused on the exploitation of artificial neural networks for modeling of the electromagnetic fields inside cars. The first part of the thesis is deals with the analytical description of electromagnetic wave propagation in the interior using Norton surface waves. In the following part, attention is turned to the practical measurement and verification of analytical models. Practical measurements were the source of training and verification data for neural networks. The thesis is focused on frequency bands 3 to 11 GHz and 55 to 65 GHz.

KEYWORDS

Artificial neural network, feed-forward network, radial basis function network, surface wave, numerical modeling of Maxwell equations, channel transfer function, localization of passengers

ABSTRAKT

Disertační práce se věnuje využití umělých neuronových sítí pro modelování elektromagnetických polí uvnitř automobilů. První část práce je zaměřena na analytický popis šíření elektromagnetických vlny interiérem pomocí Nortonovy povrchové vlny. Následující část práce se věnuje praktickému měření a ověření analytických modelů. Praktická měření byla zdrojem trénovacích a verifikačních dat pro neuronové sítě. Práce se zaměřuje na kmitočtová pásma 3 až 11 GHz a 55 až 65 GHz.

KLÍČOVÁ SLOVA

Umělá neuronová síť, dopředná síť, síť s radiální bázovou funkcí, povrchová vlna, numerické řešení Maxwellových rovnic, přenosová funkce, lokalizace pasažérů.

BIBLIOGRAFICKÁ CITACE

KOTOL, M., *Neural modeling of electromagnetic fields in cars*, Doctoral thesis. Brno: Brno University of Technology, Faculty of Electrical Engineering and Communication, Department of Radio Electronics, 2018. 72 p. Supervised by prof. Zbynek Raida.

DECLARATION

I declare that I have written the Doctoral Thesis titled “Neural Modeling of Electromagnetic Fields in Cars” independently, under the guidance of the advisor and using exclusively the technical references and other sources of information cited in the thesis and listed in the comprehensive bibliography at the end of the thesis.

As the author I furthermore declare that, with respect to the creation of this Doctoral Thesis, I have not infringed any copyright or violated anyone’s personal and/or ownership rights. In this context, I am fully aware of the consequences of breaking Regulation § 11 of the Copyright Act No. 121/2000 Coll. of the Czech Republic, as amended, and of any breach of rights related to intellectual property or introduced within amendments to relevant Acts such as the Intellectual Property Act or the Criminal Code, Act No. 40/2009 Coll., Section 2, Head VI, Part 4.

Brno, the 31st of August, 2018 …….

Author’s signature

Faculty of Electrical Engineering
and Communication
Brno University of Technology
Technická 12
616 00 Brno
Czech Republic
http://www.six-centre.cz

ACKNOWLEDGEMENT

Research described in this Doctoral Thesis has been implemented in the laboratories of the SIX Research Center, and has been supported by the project LO1401 INWITE of the National Sustainability Program.

Brno, the 31st of August, 2018 …….

Author's signature

ACKNOWLEDGEMENT

I wish to thank prof. Dr. Ing. Zbynek Raida who served as my supervisor and also encouraged and challenged me throughout my academic program.

Brno …..…… ……..

(author's signature)

ABBREVIATIONS

ANN	Artificial neural network
BER	Bit-error rate
CTF	Channel transfer function
EMC	Electromagnetic compatibility
FF	Feed-forward
LSTM	Long short-term model
LTE	Long term evolution
MISO	Multiple input single output
MLP	Multi-layer perceptron
NN	Neural network
OFDM	Orthogonal frequency division multiplexing
PAN	Personal area network
RBF	Radial basis function
RMS	Root mean square
Rx	Receive antenna
SLP	Single-layer perceptron
Tx	Transmit antenna
UWB	Ultra-wide band
VNA	Vector network analyzer
WLAN	Wireless local area network

SYMBOLS

b, b'	Phase constants
dl	Dipole length
$\mathbf{E}$	Electric field intensity
E_0	Electric field intensity of source
$\mathbf{E}_{sur}$	Vertical component of electric field intensity
$erfc$	Error function
F	Sommerfeld attenuation coefficient
f_n	Output signals of neural network
h	Threshold potential of neuron
I	Constant current
k	Wave number
m	The number of output neurons
n	The number of input neurons
p	Training set
p_1	Numerical distance
R_2	Reflection distance
R_V	Fresnel's reflection coefficient
S_{21}	Transmission between antennas
w_{mn}	Synoptic weights of neurons
x_n	Input signals of neural network
$\tilde{\varepsilon}$	Complex permittivity
ε_0	Permittivity of vacuum
ε_r	Relative permittivity
λ_0	Wavelength
ξ	Inner potential of neuron
σ	Activation function of neuron, conductivity
Ψ_1, Ψ_2	Angles

CONTENTS

CONTENT OF PICTURE

Chapter 1

Introduction

Wireless communication plays more and more important role in current technologies. Inside vehicles, wireless communication can:

- Increase the comfort. Covering the space in a vehicle by a signal, passengers can connect their personal devices into the local network to communicate, work and entertain.
- Reduce the amount of cabling. Local sensor networks can transmit collected information to central units to further processing.

From the viewpoint of current wireless technologies (mobile services, BlueTooth, ZigBee, etc.), in-car space is a very complicated environment:

- Objects in a car are comparable to wavelength. For this reason, wireless communication is influenced by those objects significantly (multiple reflections and the diffraction phenomena cannot be neglected).
- In-car environment is changeful, influenced by passengers, luggage and other objects inside.

Due to those reasons, wireless communication in a vehicle cannot be characterized deterministically, and probabilistic approaches have to be applied. Wireless communication in a car can be represented by a *channel transfer function* (CTF), and the CTF can be modeled by probabilistic approaches to simulate stochastic behavior of in-car wireless communication systems. Deterministic models do not provide a comprehensive description of related phenomena.

If a model of a CTF is going to be developed using full-wave methods (finite elements, finite differences, etc.), extreme CPU-time demands and memory requirements have to be expected due to electrically large dimensions of in-car objects. On the contrary, in-car dimensions are not large enough for asymptotic methods.

In the thesis, an alternative solution of the problem is proposed:

- First, comprehensive measurements of in-car fields for different configurations of an interior, different number of passengers and different frequencies are carried out. Since such measurements are not trivial, their validity has to be verified by numerical methods.
- Second, measured data have to be processed statistically to make them exploitable for practical use. The processed data can be used for training *artificial neural networks* (ANN) to create a black-box model of electromagnetic environment in a vehicle.

  A proper functionality of the trained network has to be carefully tested using reasonable test cases. Then, the neural model behaves like a general *approximer* providing an estimate of measured parameters even for constellations which have not been measured.

The internal structure of ANN is highly parallel. Thanks to this parallel structure, approximate responses are provided by the neural network quickly and efficiently.

For the approximation of CTF in cars, we have selected two functionally different types of neural networks – the feed-forward (FF) one and the radial basis function (RBF) one. Properties of FF ANN and RBF ANN are carefully compared for the training phase and the phase of the approximation. Methodological recommendations are formulated and verified. Development of neural black-box models of the channel transfer function corresponds with the second objective of the dissertation.

The first objective of the thesis is focused on the experimental characterization of channels in cars considering different in-car constellations, different number of passengers and different frequency bands. A proper statistical processing of measured data is a part of this objective. Methodological recommendations are expected to be formulated in this area also. The second objective, development of proper neural-network models, follows.

The dissertation thesis consists of the following parts:

- State of the art. Here, history and classification of ANN is given. Basic types of ANN are described, their structure is shown and their function is explained.

  Next, attention is turned to transmission channels in a vehicle covering frequency bands 3 GHz to 11 GHz and 55 GHz to 65 GHz.

- Objectives of the dissertation are deeply discussed. Exploitation of artificial neural networks for modeling in-car wireless communication channels is the most important contribution.

- Characterization of in-car channels is expected to provide relevant patterns for training neural networks. Patterns are obtained experimentally. Validity of experimental data is proven by simplified analytical and numerical models.

- Neural modeling of in-car channels. Conventional feed-forward neural networks and radial basis function ones are used to represent measured data. Functionality of neural models is verified, and robustness of trained networks is shown. A neural estimator of the number of passengers in a car is given as an example of an application. Exploitation of the tool in the ultra-wideband (UWB) localization is also discussed.

- Conclusion. Objectives of the thesis are focused on neural modeling of channels in cars. But the conclusion shows that the outputs of the dissertation can be generalized and applied in a variety of related problems.

Chapter 2

State of the art

The chapter consists of two parts:

- A short introduction to ANN and neural modeling is given. Attention is turned to the description of ANN, their structure, features and implementations for modeling physical phenomena.
- Electromagnetic wave propagation in vehicles is reviewed, and approaches to the analytical, numerical and experimental characterization of waves are discussed.

Exploitation of experimental data related to the in-vehicle wave propagation for building neural models of electromagnetic environment inside vehicles is the main contribution of the thesis.

2.1 Neural networks

Historical development of neural networks can be divided into three periods:

1. The birth of ANN. In 1943, W. S. McCulloch and W. Pitts [2.1] created a simple mathematical model of a neuron, and D. Hebb proposed learning rules for synapses [2.2].
2. Discovery of perceptron. The perceptron was discovered in 1957 by F. Rossenblatt [2.3]. This discovery started the theoretical and practical development of ANN. But unfortunately, the research of ANN gradually weakened since computational technology was not developed sufficiently that time.

   As an imaginary end of the second period, the year 1969 can be regarded when the monograph on perceptrons, which was authored by Minsky and Papers [2.4], was published.
3. Renewed interest in ANN. In 1982, J. Hopfield renewed the interest of the scientific community in ANN. Due to the increasing power of computers, the development of ANN has been continual since that time

The similarity of ANN with biological neural networks enables us to solve various problems: ANN can optimize, predict, control, manage, etc. [2.5]. These problems can be alternatively solved by conventional approaches but the conventional solution can be inflexible, time-consuming and computationally demanding.

The ANN consists of simple computing units, called the neurons. McCulloch and Pitts presented the first model of a neuron in [2.1]. This model had one or more inputs. Input signals were weighted by synoptic weights, weighted signals were summed and processed by a non-linear activation function. That way, the output signal of the neuron was created. The output signal of the neuron was equal to 1 if the sum of input signals exceeded a threshold value. Otherwise, the output signal of the neural model was 0.

The structure of a general neuron is show in Figure 2.1 [2.5], [2.6]:

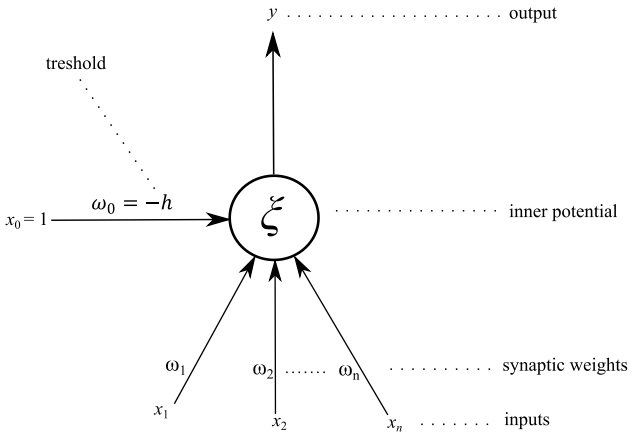

Figure 2.1: Structure of general neuron

The general neuron has n a general inputs $x_1, \ldots, x_n$. Each input is associated to a corresponding synaptic weight $w_1, \ldots, w_n$. The synaptic weights correspond to the strength of a synopsis of a real biological neuron. Synoptic weight are weakened or strengthened during the process of learning. That way, information is stored in the neuron [2.5], [2.6].

The sum of weighted inputs corresponds to the inner potential of the neuron [2.5], [2.6]

$$\xi = \sum_{i=1}^{n} w_i x_i \tag{2.1}$$

Here, w_i is the ith synoptic weight, x_i is the ith input signal and n is the number of inputs of the neuron.

When value of the inner potential ξ reaches a threshold h, the output of the neuron y is activated. The output value $y = \sigma(\xi)$ is influenced by the non-linear activation function σ. The sharp nonlinearity is the simplest type of the activation function to be used [2.5], [2.6]

$$\sigma(\xi) = \begin{cases} 1 \;\; if \;\; \xi \geq h \\ 0 \;\; if \;\; \xi < h \end{cases} \tag{2.2}$$

The unipolar sigmoidal function and the bipolar sigmoidal function belong to other most frequently used activation functions.

In the open literature, even more advanced models of neurons have been presented. For example, the multiplicative model of the neuron was based on a polynomial architecture, and was exploited to solve a large range of problems [2.7].

Now, let us move from a single neuron to a neural network.

In the human brain, neurons are organized into layers which are mutually interconnected and create a network. An internal connection of neurons into the network associates the input of each neuron in the layer M with outputs of neurons in the previous layer $M - 1$. The output of the neuron in the layer M is connected to all the inputs of neurons in the next layer $M + 1$. Individual neurons are interconnected by synoptic weights [2.5], [2.6].

As already mentioned, neurons are organized in layers. The ANN can contain three basic types of the layers – the input layer, the hidden layer, and the output layer:

- The input layer distributes signals to the next layer;
- The hidden layer processes signals;
- The output layer forms the output signal.

The ANN is characterized by the ability to learn. During the learning process, connection between individual neurons are amplified or weakened until the mean square error falls below the prescribed level and the output of the network corresponds with the input values in the desired manner [2.5], [2.6].

From the viewpoint of working activity, three modes of operation of ANN can be defined [2.5], [2.6]:

- The mode of organization is related to creating topology of ANN

  When creating ANN, decision on the type of the network (feed-forward, recurrent, cellular) has to be done, the optimal number of neurons has to be selected, and the optimal organization of neurons has to be chosen (the number of layers, and the number of neurons in layers).

- The mode of adaptation (training)

  At the beginning of training, synoptic weights are set randomly usually. During the training process, input patterns are introduced to inputs of ANN, and outputs of ANN are compared with output targets. Synoptic weights are iteratively changed to minimize the difference between ANN outputs and output targets.

- The mode of activity

  After finishing the training, unknown signals are introduced to inputs of ANN, and the network forms output responses using experience learned during the training process.

ANN can be applied in modeling of stochastic phenomena also. In the literature, only few publications related to this problem are available [2.8], [2.9]. In the thesis, neural modeling of stochastic phenomena will be applied on the development of a *channel transfer function* (CTF) for wireless communication in the interior of a car.

Let us turn the attention to the mode of organization. In Figure 2.2, the most frequently used ANN architectures are shown. Cyan circles symbolize neurons (Figure 2.1). In the following text, we deal with architectures which are relevant for modeling of in-car communication only.

Historically, the first model of the ANN was the single-layer perceptron network [2.3]. The network architecture of perceptron contains a single layer of neurons. The network consists of n input neurons. Outputs of input neurons are inputs of each of the m output neurons. Output of the perceptron has the shape of a sharp nonlinearity, and produces a value of 1 or 0, depending on the configuration of weights w.

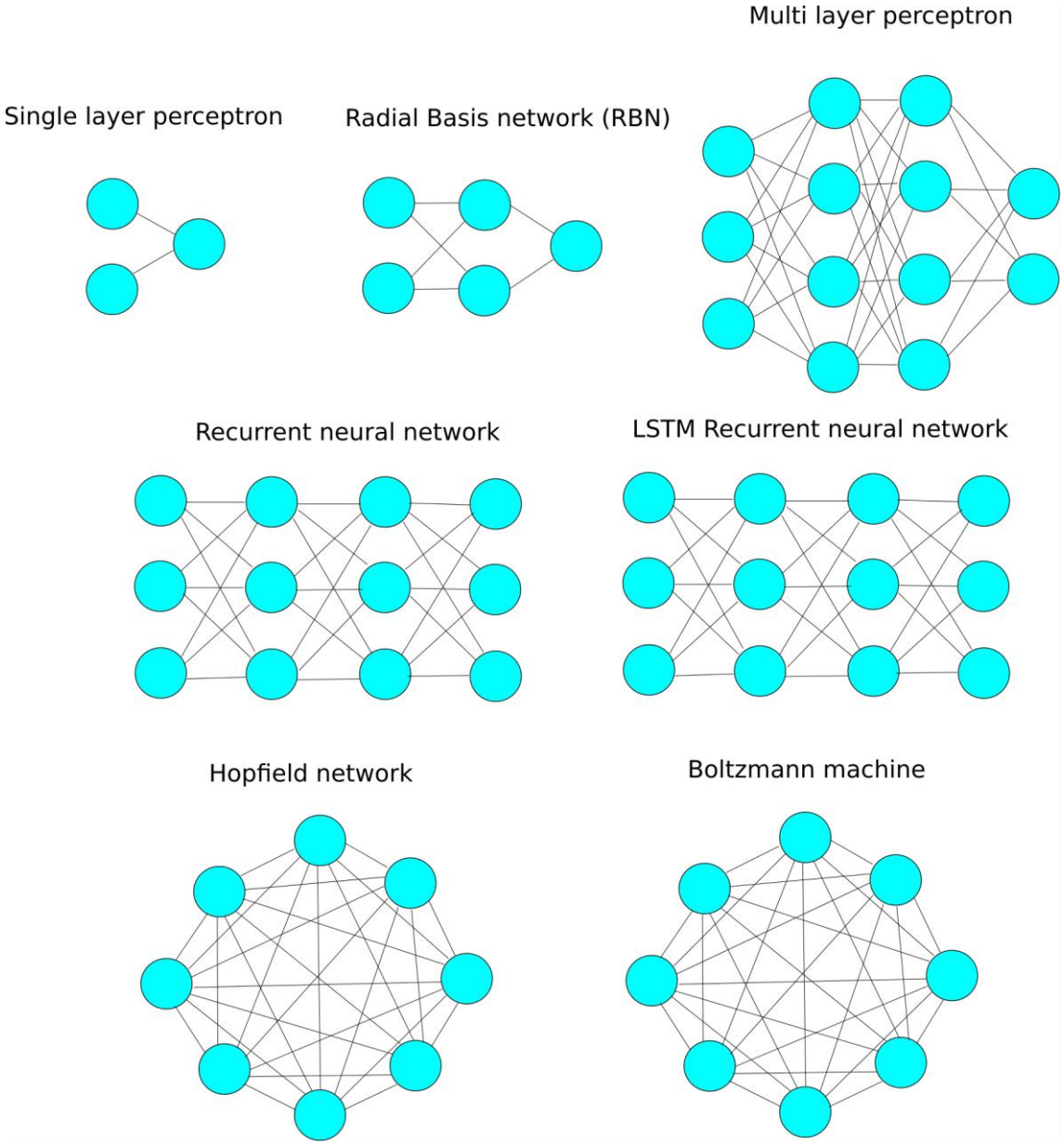

Figure 2.2: Architectures of artificial neural networks (ANN)

The multilayer perceptron is the most widely used ANN. The multilayer ANN is trained by the learning algorithm based on the back-propagation of the error [2.10]. Usually, a two-layer or a three-layer topology of the network is used. The topology is fixed before training. Non-linearity in neurons is usually of the form of a sigmoidal function. Weights are set randomly. During training, weights are determined so that the output of the network matches targets corresponding to related input patterns. Since the input signal propagates from the input of the network to its output, the multi-layer perceptron is also called *feed-forward artificial neural network* (FF ANN).

The Hopfield network is another important model of the ANN. Hopfield [2.11] when analyzing the stability of the network used the analogy of a physical theory of the magnetic

materials, and thanks to this, the network model became widely known. The organizational structure of the network is specified at the beginning of the solid topologies network with *n* neurons. The neurons are connected in the network each with each, and all neurons in the network are input ones and output ones. Training of the Hopfield network is specified by a training set *p*. During network training, training patterns are presented to the network, and synaptic weights are adapted until the output values match the values of the input function.

The model of the ANN proposed by Hinton and Sejnowski [2.12], [2.13] is called the Boltzmann machine. Organizing the network is specified at the beginning and has a fixed architecture. The symbol *n* denotes input neurons, *b* hidden neurons and *m* output neurons. The input neurons are set by the input data values and the hidden neurons are set randomly at the start of the active mode. Training of the network is similar to the Hopfield network.

The radial basis function (RBF) ANN [2.14] belongs among the major ANN. The RBF network is a three-layer network. Input neurons are used for transferring input values. The second (hidden) layer implements the radial functions to input values. The third layer is the output one and forms output targets.

The hidden neuron has *n* inputs. Each input has an associated weight and has one output. The RBF activation function is different from others; the internal potential is not calculated as a scalar product but as the distance of input values from the RBF function. During training, training patterns are presented to the network to adapt synaptic weights until the output values match the values of the input function. The output values are formed by output neurons which calculate the weighted sum of its inputs [2.14].

Finally, let us turn the attention to the training of neural networks.

Let us consider the FF ANN containing three layers of neurons (the input layer, the hidden layer and the output layer) [2.14]. The hidden layer can be divided to three sub-layers (maximally). The topology of the FF ANN has to be fixed at the beginning.

The input layer distributes the input signal among hidden neurons [2.14]. Neurons in hidden layers transform signals using a specific activation function. The output layer forms output targets (Figure 2.3). Here, x_1 to x_n are signals at the input of input neurons, w_{11} to w_{mn} denote weights between neurons and f_1 to f_n are signals at the output of output neurons.

FF ANN uses the forward spread of information: information flows in one direction without any feedback. At the beginning of training, weights between neurons are set randomly. During training, weights are set such a way to minimize the difference between expected outputs and current ones. The difference between expected outputs and current ones, i.e. the error, propagates from the output to the input so that synoptic weights could be updated accordingly. The training is therefore called back propagation.

The RBF ANN consists of the input layer, the hidden layer and the output layer as well. The input layer transmits input signals to neurons in the hidden layer again. The hidden layer transforms signals by the Gauss kernel function: signals close to the center of the Gauss kernel function are amplified, and conversely [2.5], [2.6]. The output layer contains output neurons described by a linear function. Output neurons take care for forming the output patterns. The

general structure of the RBF network is shown in Figure 2.4. Here, x_1 to x_n are signals at the input of input neurons, w_{11} to w_{mn} denote weights between neurons and f_1 to f_n are signals at the output of output neurons.

When training RBF ANN, all training patterns are associated with a new network. Then, the *mean square error* (MSE) is calculated. According to MSE values, we set thresholds and weights between neurons in order to reduce the MSE values. The procedure is repeated until the MSE drops below a predetermined value.

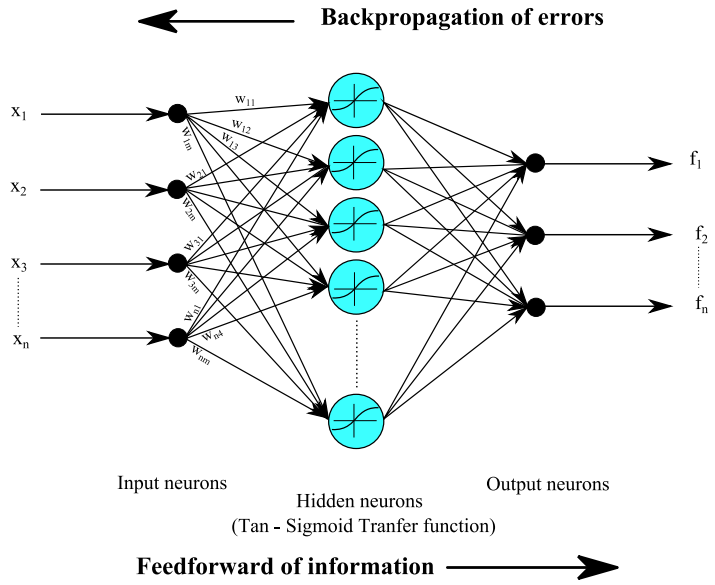

Figure 2.3: Architecture of FF ANN.

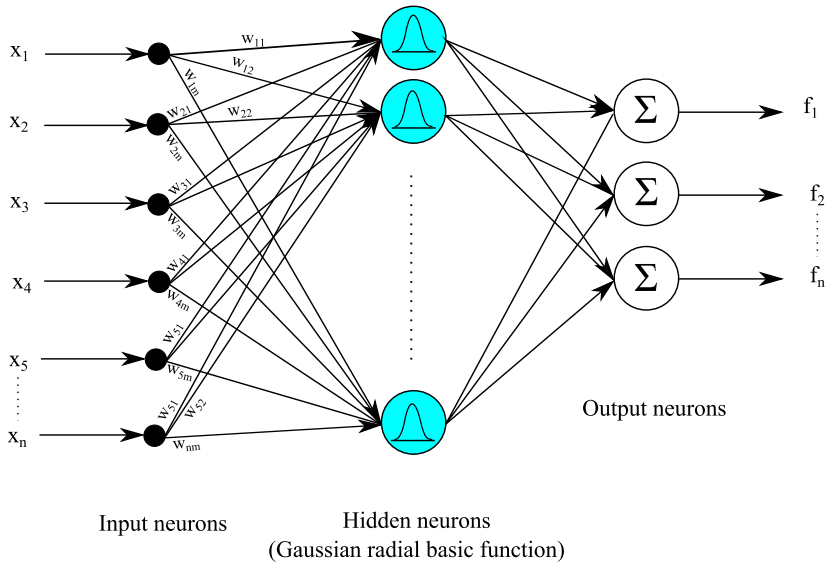

Figure 2.4: Architecture of RBF ANN.

ANN can solve problems where conventional sequential algorithms fail. The ANN can be used if satisfactorily large training sets are available.

The ANN can be also used for the solution of electromagnetic compatibility (EMC) problems. In [2.16], the author describes modeling of small aircraft using ANN. The author focuses on the use of ANN in terms of a high-performance computing and accelerates modeling because classical EMC methods are time-consuming.

Modeling of CTF characteristics is a computationally consuming task also [2.17]. In [2.17], the author estimates the loss of the CTF in mines. Input patterns consisted of the frequency and the distance between transmitting and receiving antennas. UWB frequency band was from 3.1 GHz to 10.6 GHz.

In [2.18], the back propagation ANN and the RBF ANN are used to estimate impulse responses of a channel of the OFDM system. The input pattern was created by the real and the imaginary part of the signal. For estimating the channels of the downlink of the LTE system, ANN has been used too [2.19]. The ANN estimated a suitable channel for downlink from the parameters of OFDM pilot channels.

Several approaches to the exploitation of ANN for the modeling of wireless propagation channels have been described in the open literature:

- In [2.20], authors showed an approach to the modeling of the propagation delay and the atmosphere parameters such as humidity, pressure, and temperature. Attention was turned to the propagation factors affecting the wireless channel in the frequency range from 300 MHz to 100 GHz. Authors used a multilayer perceptron.

- In [2.21], ANN was used for predicting future spectrum holes to save energy of spectrum sensing and to improve the efficiency of spectrum access. The author exploited a back propagation ANN which predicted the future spectrum holes form a channel power value.

- In [2.22], ANN was used for modeling satellite communication channels. The model was based on a multi-layer ANN which was trained by the back propagation algorithm.

- In [2.23], ANN was applied to modeling a multi-path indoor channel. The ANN was asked to estimate the impulse response and transmission multi-path indoor channel. The neural estimator used a multilayer perceptron.

- In [2.24], the ANN was used for modeling wireless channel from modulated I and Q signals. From the analysis, ANN estimated important channel parameters (number multi-path, Doppler frequency shift, time lag, etc.).

Previous paragraphs show possible ways of modeling wireless channels supported by ANN. In the following paragraphs, we will show approaches to the modeling of wireless channels without ANN:

- In [2.25], several approaches to the modeling of inner UWB (3.1 GHz to 10.6 GHz) channels in moving cars are shown. A stochastic model and statistical parameters of the channel were derived from the data measured in a stationary vehicle and a moving one.

- The paper [2.26] presents an ultra-wideband (UWB) channel measurement and modeling for an intra-vehicle environment. Measurement and processing according to the position of the transmit antenna and the receive one in a car were investigated in [2.27].

- The simple and robust model characterizing the frequency dependent transfer function of an in-vehicle ultra-wide-band channel was described in [2.28].

- A short range channel for indoor wireless applications operating at 60 and 70 GHz was measured and modeled in [2.29]. Here, authors described a transmit channel in time domain and frequency domain for the environment of an office, a shopping mall and a station. Transmission between the transmitting antenna and the receiving one was measured when changing the range and the direction of the transmit antenna.

- In [2.30], [2.31], [2.32], a statistical channel model for indoor 60 GHz WLAN propagation channel was published. The proposed model provided an accurate space-time characteristics of the propagation channel, supported beamforming with steerable antennas, and polarization characteristics of antennas and signals. The methodology was used by the channel modeling group of the IEEE 802.11ad standardization, working on the design of the specification for next generation 60 GHz WLAN systems.

- The paper [2.33] described modeling of an indoor channel according to the effect of human activity. Authors presented an analytical expression for the conditional bit-error-rate (BER) performance, conditioned on the channel, for the multiuser and single-carrier system.

In the literature, there are not many publications related to the measurement and modeling CTF in cars. This issues are addressed in [2.34], [2.35] where a comparison of UWB (3 to 8 GHz) channels inside three different car types is carried out for several scenarios with the variety of existing passenger and different positions of antennas. The delay spread and the maximum excess delay are derived. The variation of such parameters is investigated for different car geometries and antenna positions.

In [2.36], authors compare measurement of a UWB channel and a 60 GHz channel in a car. The comparison between an occupied car and an empty car shows that passengers have to be included in the planning process for 60 GHz as well as for UWB in-car systems.

2.2 Characterization of In-car Channels

The CTF in a car is affected by a large number of phenomena. These phenomena are quasi-static and dynamic:

- Quasi-static phenomena are stable over the time or change very slowly. The time-invariant phenomena are related to the shape of internal body of a car, the placement and adjustment of seats, etc.

- Dynamic phenomena are changed in time often and very quickly. As the dynamic phenomenon, we can classify phenomena related to the crew in the car which moves during the journey.

The stochastic process is defined as a set of random variables within a certain probability space at certain time. The analysis of stochastic phenomena is described in [2.8] including a unified approach to solve stochastic problems.

More effective analysis of stochastic processes is provided by the method of scale-recursive structures [2.9]. This algorithm allows systematic estimate and reconstruction of the signals. In [2.9], the author describes a standard analytical Gaussian Markov tool. This tool allows us to analyze more dimensional signals but this technique relies heavily on the singular decomposition value, which can be computationally consuming.

The analysis of the stochastic phenomena can be quite computationally extensive. To reduce computational demands, artificial neural structures can be used to form a parallel high-performance computing network which is able to learn and adapt.

Modern automobiles contain a multitude of wireless transmission systems for mobile telephony, in-car communication, car-to-x communication, etc. The characterization of the wireless transmission environment and verification of these complex systems, which connect the acquisition of information with the operational status of cars, passengers and other traffic participants and their environment, raise requirements on reliable techniques for electromagnetic measurements and system performance evaluation.

The rapid development of wireless technique shows a strong trend towards intelligent connected vehicles and further advances in automation of driving functions. In future automobiles, wireless systems for communications and sensing will play an even more crucial role than today. Reliable wireless links become indispensable. Thus, we can ensure quality a numerical models and followed by detailed measurements for verify a numerical models [2.37].

Attention is turned to creating small communication networks inside a car, or developing car-to-car networks which provide wireless connectivity between vehicles on the one hand and between vehicles and the infrastructure on the other hand. Car-to-X communications are currently being researched and developed to increase traffic safety and efficiency in order to provide improved convenience to the driver. This also leads to the migration of wireless systems into the car [2.38].

Papers [2.37], [2.38] are focused on high frequencies in the bandwidth 60 GHz. Currently, devices (transmitters, receivers, antennas) are too expensive for massive using in the automotive industry, and therefore, the UWB (3 to 11 GHz) seems to be more promising from an application point of view. A comparison of ultra-wideband (UWB) and 60 GHz channels inside a car is provided in [2.36]. In this study, measured attenuation between the transmit and receive antennas in deferent locations in a car are compared in detail in UWB and at 60 GHz.

Similar measurements in a bus are discussed in [2.39]. In [2.40], [2.41], real-word measurements of the wireless intravehicular channel are provided for bands 3 to 11 GHz and

55 to 65 GHz under similar conditions inside a car. In both situations, the power-delay profile is obtained by spatially averaging of channel impulse response realizations within the grid of 10×10 antennas. Data measured in bands 3 to 11 GHz and 55 to 65 GHz show significant differences in terms of the root mean square (RMS) delay spread, the number of resolvable clusters, and the variance of the maximal excess delay. The measured and calculated results indicate that a strong reverberation inside the vehicle produces a similar power-delay profile within the range of approximately ten wavelengths.

A dynamic channel measurement in a car is described in [2.42]. Analysis of measured data discovered that effects of a running engine or a loudly playing built-in audio system are negligible in comparison with the influence of a car body vibration or twisting caused by the motion of the car. Moreover, movements of passengers in the car-cabin, driving the car on a bumpy road, accelerating and braking are considerable effect on the channel time variance.

Both large-scale parameters and small-scale ones can be investigated by measurement and modeling. In this context, locations of the transmit antenna and receive one, and the difference between an empty car and a fully occupied one was explored in the time domain and the frequency domain [2.43].

Next, the multiple input single output (MISO) channel can be measured in the UWB frequency band. The measurements were performed in a mid-sized passenger car with transmit and receive antennas. This experiment was aimed to investigate a small shift (less than wavelength) of the receive antenna within 10×10 spatial points placed on the board. The spatial channel stationary evaluated in terms of correlation coefficients between absolute values of measured channel impulse response were published in [2.44].

The extensive UWB measurement campaign in three different car types for several scenarios is descripted in [2.34]. From the measurement results, channel parameters such as path loss, RMS delay spread and maximum excess delay are derived. The variation of such parameters is investigated for different car geometries and antenna positions. For creating a reliable UWB channel, a wide range of parameters (path loss, RMS delay spread and maximum excess delay) has to be considered.

The roof of a car can be used for communication in inside the car. The study [2.45] shows the effect of the surface wave on the transmission between the antennas in case of different surfaces (metal, carbon, 3D textile, etc.). The 3D textile is the most influential on the transmission coefficient because is suitable for creation of a transmission line in the 60 GHz ISM band.

2.3 Conclusions

The *State of the Art* results in following conclusions:

- Research of electromagnetic wave propagation in vehicles is topical. In IEEE Xplore and other professional databases, several papers on measurement and modeling of vehicular wireless channels have been published currently.
- Measurements of wireless communication channels in the UWB frequency band and the 60 GHz ISM band have been described in the open literature already. Nevertheless, outputs of measurements have not been verified by appropriate numerical modeling and approximate analytical models yet. Moreover, transformation of the measured data into training sets for learning neural networks has not been published yet.
- Methodology of a neural training of in-vehicle wireless communication channels based on extensive measurements, simulations and analytical modeling has not been described in the open literature sufficiently yet.

Considering these conclusions, objectives of the dissertation thesis are formulated in the following chapter.

2.4 References

[2.1] W. S. McCulloch and W. Pitts, A logical calculus of the ideal immanent in nervous activity, *Bulletin of Mathematical Biophysics*, no. 5, p. 115-133, 1943.

[2.2] D. O. Hebb, *The Organization of Behavior: A Neuropsychological Theory*, Wiley, New York, 1949.

[2.3] F. Rossenblatt, The perceptron: a probabilistic model for information storage and organization in the brain, *Psychological Review*, no. 65, p. 386-408, 1958.

[2.4] M. L. Minsky and S. A. Papert, *Perceptrons*, MIT Press, Cambridge, 1969.

[2.5] S. Haykin, *Neural Networks and Learning Machines*, 3/E, Prentice Hall, Englewood Cliffs, 2008.

[2.6] J. Šíma and R. Neruda, *Teoretické otázky neuronových sítí* (in Czech), Matfyzpress, Praha, 1996.

[2.7] R. N. Yadav, P. K. Kalra, and J. John, Time series prediction with single multiplicative neuron model, *Applied Soft-Computing*, no. 7, p. 1157–1163, 2007

[2.8] I. Iavorskyj and V. Mykhajlyshyn, Probabilistic analysis of electromagnetic phenomena with stochastic periodicity, *International Conference on Mathematical Methods in Electromagnetic Theory*, Lviv: IEEE, p. 252-255, 1996.

[2.9] W. W. Irving, W. C. Karl and A. S. Willsky, A theory for multiscale stochastic realization, *IEEE Conference on Decision and Control*, Lake Buena Vista, p. 655-662, 1994.

[2.10] D.E. Rumelhart, G.E. Hinton and R.J. Williams, Learning internal representations by error propagation. *Parallel Distributed Processing: Explorations in the Micro-structure of Cognition*, MIT Press, Cambridge MA, vol. 1, p. 318-362, 1986.

[2.11] J.J. Hopfield, Neural networks and physical systems with emergent collective computational abilities, *Proceedings of the National Academy of Sciences*, vol. 79, p. 2554-2558, 1982.

[2.12] G. E. Hinton and T.J. Sejnowski, Optimal perceptual inference, *IEEE Conference on Computer Vision and Pattern Recognition*, Washington, p. 448 – 453, 1983.

[2.13] G. E. Hinton and T. J. Sejnowski, Learning and relearning in Boltzmann machines. *Parallel Distributed Processing: Explorations in the Microstructure of Cognition*, MIT Press, Cambridge MA, vol. 1, p. 282-317, 1986.

[2.14] D. Kriesel, *A Brief Introduction to Neural Networks*, University of Bonn, available: http://www.dkriesel.com, 2007

[2.15] Jingwen Tian, Meijuan Gao and Fan Zhang, Network intrusion detection method based on radial basis function neural network, *International Conference on E-Business and Information System Security*, 2009.

[2.16] V. Koudelka, *Probabilistic neural networks for special tasks in electromagnetics*. Doctoral thesis, Brno University of Technology, 2014.

[2.17] N. Zaarour, N. Kandil and N. Hakem, An accurate neural network approach in modeling an UWB channel in an underground mine, *Antennas and Propagation Society International Symposium*, IEEE, Orlando, p. 1608-1609, 2013.

[2.18] N. Taşpinar and M. N. Seyman, Back propagation neural network approach for channel estimation in OFDM system, *International Conference on Wireless Communications, Networking and Information Security*, IEEE, Beijing (China), p. 265-268, 2010.

[2.19] A. Omri, R. Hamila, M. Hasna, R. Bouallegue and H. Chaieb, Estimation of highly selective channels for downlink LTE system by a robust neural network, *International Conference on Communication in Wireless Environments and Ubiquitous Systems: New Challenges*, Sousse, 2010.

[2.20] T. Moazzeni, A wireless propagation channel model with meteorological quantities using neural networks, *IEEE Consumer Communications and Networking Conference*, p. 1307-1309, 2006.

[2.21] S. Bai, X. Zhou and F. Xu, Spectrum prediction based on improved-back-propagation neural networks, *International Conference on Natural Computation*, Zhangjiajie, p. 1006-1011, 2015.

[2.22] M. Ibnkahla and F. Castanie, Neural network identification of digital satellite channels: the adaptive nonlinear enhancer, *International Conference on Neural Networks*, IEEE, Washington, p. 1628-1633, 1996.

[2.23] Yong-Tao Ma, Kai-Hua Liu and Yi-Na Guo, Artificial neural network modeling approach to power-line communication multi-path channel, *International Conference on Neural Networks and Signal Processing*, Nanjing, p. 229-232, 2008.

[2.24] L. Lv, A novel wireless channel model with multiply feed-forward neural network, *Third International Conference on Natural Computation*, Haikou, p. 730-734, 2007.

[2.25] J. Ren, C. Cai, H. Zhao and Z. Xie, Research and simulation analysis of UWB indoor channel model, *International Conference on Computer Science & Service Systems*, Nanjing, p. 1228-1231, 2012.

[2.26] W. Niu, J. Li and T. Talty, Intra-vehicle UWB channels in moving and stationary scenarios, *Military Communications Conference*, IEEE, Boston, 2009.

[2.27] M. Schack, J. Jemai, R. Piesiewicz, R. Geise, I. Schmidt and T. Kurner, Measurements and analysis of an in-car UWB channel, *Vehicular Technology Conference* (VTC Spring 2008), IEEE, Singapore, p. 459-463, 2008.

[2.28] A. Chandra; A. Prokes; T. Mikulasek; J. Blumenstein; P. Kukolev; T. Zemen; C. F. Mecklenbrauker, Frequency-domain in-vehicle UWB channel modeling, *IEEE Transactions on Vehicular Technology*, 2016, vol. 65, no. 6, p. 3929-3940.

[2.29] K. Haneda, J. Järveläinen, A. Karttunen, M. Kyrö and J. Putkonen, A statistical spatio-temporal radio channel model for large indoor environments at 60 and 70 GHz, *IEEE Transactions on Antennas and Propagation*, vol. 63, no. 6, p. 2694-2704, 2015.

[2.30] A. Maltsev, R. Maslennikov, A. Sevastyanov, A. Lomayev and A. Khoryaev, Statistical channel model for 60 GHz WLAN systems in conference room environment, *Fourth European Conference on Antennas and Propagation*, Barcelona (Spain), 2010.

[2.31] D. Cassioli, 60 GHz UWB channel measurement and model, *International Conference on Ultra-Wideband*, IEEE, Syracuse, p. 145-149, 2012.

[2.32] L. Clavier et al., Wide band 60 GHz indoor channel: characterization and statistical modeling, *Vehicular Technology Conference* (VTC Fall 2001), IEEE, Atlantic City, p. 2098-2102, 2001.

[2.33] T. V. Nguyen, E. Masry and L. B. Milstein, Channel model and performance analysis of QAM multiple antenna systems at 60-GHz in the presence of human activity, *Global Telecommunications Conference*, IEEE, Houston, 2011.

[2.34] M. Schack, R. Geise, I. Schmidt, R. Piesiewiczk and T. Kurner, UWB channel measurements inside different car types, *Third European Conference on Antennas and Propagation*, Berlin, p. 640-644, 2009.

[2.35] M. Schack, J. Jemai, R. Piesiewicz, R. Geise, I. Schmidt and T. Kurner, Measurements and analysis of an in-car UWB channel, *Vehicular Technology Conference* (VTC Spring 2008), IEEE, Singapore, p. 459-463, 2008.

[2.36] M. Schack, M. Jacob and T. Kurner, Comparison of in-car UWB and 60 GHz channel measurements, *Fourth European Conference on Antennas and Propagation*, Barcelona, Spain, 2010.

[2.37] F. Wollenschläger, P. Berlt, C. Bornkessel and M. A. Hein, Antenna configurations for over-the-air testing of wireless automotive communication systems, *Tenth European Conference on Antennas and Propagation*, Davos, Switzerland, 2016.

[2.38] M. Blesinger et al., Angle-dependent path loss measurements impacted by car body attenuation in 2.45 GHz ISM Band, *Vehicular Technology Conference* (VTC Spring 2012), Yokohama, 2012.

[2.39] A. Chandra, T. Mikulasek, J. Blumenstein and A. Prokes, 60 GHz mmW channel measurements inside a bus, *8th IFIP International Conference on New Technologies, Mobility and Security* (NTMS 2016), Larnaca, Cyprus, 2016.

[2.40] J. Blumenstein et al., In-vehicle channel measurement, characterization, and spatial consistency comparison of 3-11 GHz and 55-65 GHz frequency bands, *IEEE Transactions on Vehicular Technology*, 2017, vol. 66, no. 5, p. 3526-3537.

[2.41] J. Vychodil, J. Blumenstein, T. Mikulasek, A. Prokes and V. Derbek, Measurement of in-vehicle channel: Feasibility of ranging in UWB and MMW band, *International Conference on Connected Vehicles and Expo* (ICCVE 2014), Vienna, Austria,, 2014, p. 695-698.

[2.42] A. Prokes, J. Vychodil, M. Pospisil, J. Blumenstein, T. Mikulasek and A. Chandra, Time-domain nonstationary intra-car channel measurement in 60 GHz band, *International Conference on Advanced Technologies for Communications* (ATC 2016), Hanoi, Vietnam, 2016.

[2.43] M. Schack, J. Jemai, R. Piesiewicz, R. Geise, I. Schmidt and T. Kurner, Measurements and analysis of an in-car UWB channel, *Vehicular Technology Conference* (VTC Spring 2008), Singapore, 2008, p. 459-463.

[2.44] T. Sanpechuda and L. Kovavisaruch, A review of RFID localization: Applications and techniques, *Electrical Engineering/Electronics, Computer, Telecommunications and Information Technology Conference*, (ECTI-CON 2008), Krabi, Thailand, 2008, p. 769-772.

[2.45] J. Vélim, Z. Raida, J. Láčík, J. Lambor and M. Kotol, On-roof wireless link operating at 60 GHz, *IEEE-APS Topical Conference on Antennas and Propagation in Wireless Communications* (APWC 2015), Turin, Italy, 2015, p. 153-156.

Chapter 3

Objectives

The previous chapter briefly summarizes state of the art in the area of neural modeling on in-car wireless channels. Considering outputs of this summary, two objectives of the dissertation can be formulated.

Objective 1

Methodology of experimental characterization of wireless channels in vehicles will be worked out with the emphasis on the exploitation of measured data for the training of artificial neural networks. The CTF in the interior of a car will be experimentally characterized in frequency ranges from 55 GHz to 65 GHz and from 3 GHz to 11 GHz. Validity of selected measurements will be verified by simulations in proper software and approximate analytical models.

Objective 2

Methodology of the approximation of outputs of in-car measurements by artificial neural networks will be worked out. Neural approximations will be investigated from the viewpoint of an optimally architecture of the network, convergence of the training process, an optimal composition of training sets and a proper validation. Neural models will be developed for various in-car applications (statistical characterization of channel transfer functions, identification of objects in a car, etc.).

Chapter 4

Characterization of transmission channels

The chapter is aimed to describe wireless channels in cars in a very simple way. Simplified descriptions are necessary for the verification of experimental and numerical data.

This task can be divided into two sub-tasks: propagation along the conductive surface of a car, and a multi-path propagation in the empty space in a car. For simplicity, let us consider the surface wave.

In order to represent the surface of a car simply, electrically conductive metal plate is considered. Then, the wave propagating along the surface can be considered being the Norton wave [4.1]. The analytical description based on the Norton surface wave can be compared with the numerical model developed in CST Microwave Studio.

4.1 Surface waves

The energy radiated from a transmitter can be received on a receiver side after propagation over many possible paths. In a car, three mechanisms of electromagnetic wave propagation can be distinguished:

- The direct wave propagating along the line of sight between a transmitter and a receiver;
- The reflected wave created by reflections from surfaces inside the car. The reflected wave can be characterized by the reflection coefficient R_v.
- The surface wave propagating along the interface between the metallic body of a car and air inside. The surface wave can be represented by the Norton wave [4.1].

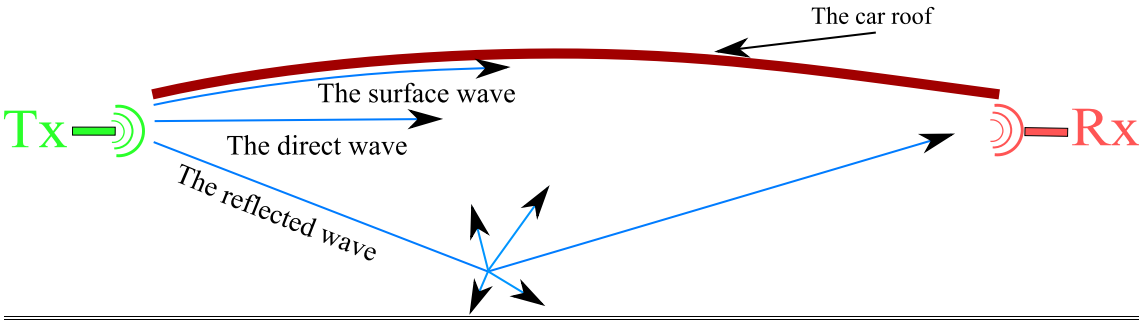

Figure 4.1: Mechanisms of electromagnetic wave propagation in a car [4.1].

The far field electric field intensity E_z (the vertical component) of the vertical Hertz dipole of the length *dl* and the constant current *I* can be expressed as [4.1]:

$$E_z = j\ 30\ k\ I\ dl \begin{bmatrix} \cos^2\Psi_1\ \frac{e^{-jkR_1}}{R_1} + R_V\ \cos^2\Psi_2\ \frac{e^{-jkR_2}}{R_2} + \\ +(1+R_V)(1-u^2+u^4 cos^2\Psi_2)\ F\ \frac{e^{-jkR_2}}{R_2} \end{bmatrix} \tag{4.1}$$

The expression (4.1) assumes the vertical dipole being situated in free space (vacuum) above a half-space created by a lossy dielectric (see Figure 4.2). The total field is a superposition of the direct wave, the reflected wave and the surface wave.

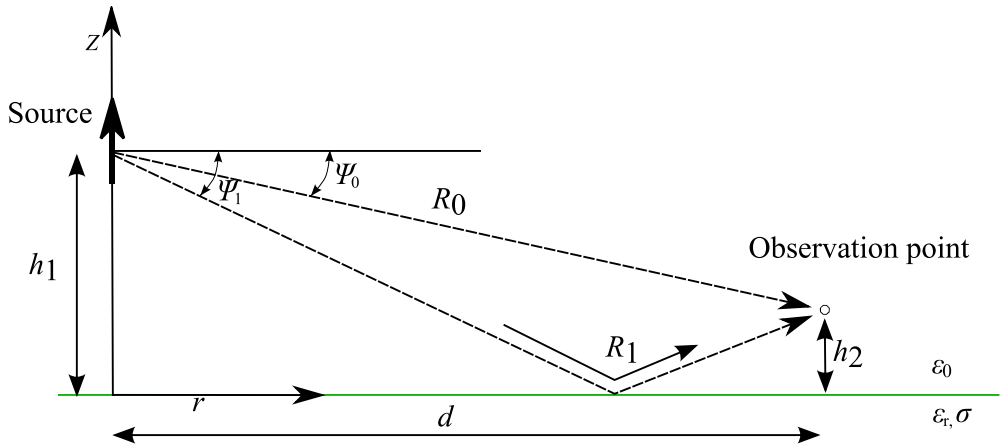

Figure 4.2: The spatial wave as a superposition of the direct wave and a reflected wave.

In (4.1), k is wave number in vacuum, angles Ψ_1 and Ψ_2 are depicted in Figure 4.2, R_1 and R_2 are trajectory lengths of the direct wave and the reflected one between the transmitter and the receiver, R_V denotes the Fresnel coefficient [4.1]

$$R_V = \frac{\widetilde{\varepsilon_r} sin\Psi - \sqrt{\widetilde{\varepsilon_r} cos^2\Psi}}{\widetilde{\varepsilon_r} sin\Psi + \sqrt{\widetilde{\varepsilon_r} cos^2\Psi}} \tag{4.2}$$

u is the parameter given by [4.1]

$$u^2 = \frac{1}{\widetilde{\varepsilon_r}} \tag{4.3}$$

$\tilde{\varepsilon}$ is the complex relative permittivity [4.1]

$$\tilde{\varepsilon} = \varepsilon - j\frac{\sigma}{\omega} = \varepsilon_0\varepsilon_r - j\frac{\sigma}{\omega} = \varepsilon_0\left(\varepsilon_r - j\frac{\sigma}{\omega\varepsilon_0}\right) = \varepsilon_0\widetilde{\varepsilon_r} = \varepsilon_0(\varepsilon_r - j\ddot{\varepsilon}_r) \tag{4.4}$$

ε_0 is permittivity of vacuum, ε_r is relative permittivity, σ is conductivity, $\ddot{\varepsilon}_r$ is complex part of relative permittivity and F is the Sommerfeld attenuation coefficient [4.1]

$$F = \left\{1 - i\sqrt{\pi p}\ e^{-p}\ erfc\left(i\sqrt{p}\right)\right\} \tag{4.5}$$

p_1 is the numerical distance and *erfc* is the error function defined by [4.1]

$$erfc\left(j\sqrt{p_1}\right) = \frac{2}{\sqrt{\pi}}\int_{j\sqrt{p_1}}^{\infty} e^{-v^2}\ dv \tag{4.6}$$

with v being the auxiliary constant of integration.

Attenuation of the Norton surface wave depends on the numerical distance p_1, electrical parameters of the surface and heights of antennas. The numerical distance for the horizontal polarization and the vertical polarization are described by [4.1]:

$$p_V = |p_{1,V}| = \frac{\pi d}{\lambda_0 \ddot{\varepsilon}_r} cosb \tag{4.7}$$

$$p_H = |p_{1,H}| = \frac{\pi d \ddot{\varepsilon}_r}{\lambda_0} \frac{1}{cosb'} \tag{4.8}$$

where λ_0 is the free-space wavelength and b, b' are phase constants [4.1]:

$$b = tan^{-1} \frac{\varepsilon_r + 1}{x} \tag{4.9}$$

$$b' = tan^{-1} \frac{\varepsilon_r - 1}{x} \tag{4.10}$$

Figure 4.3 shows the dependence of the Sommerfeld attenuation coefficient on the distance between the transmit antenna and the receive one (0.2 m to 2.0 m). For the calculation, ISM frequency bands at 2.4 GHz, 5.8 GHz and 60 GHz were selected. The dependencies demonstrate differences between the vertical polarization and the horizontal one.

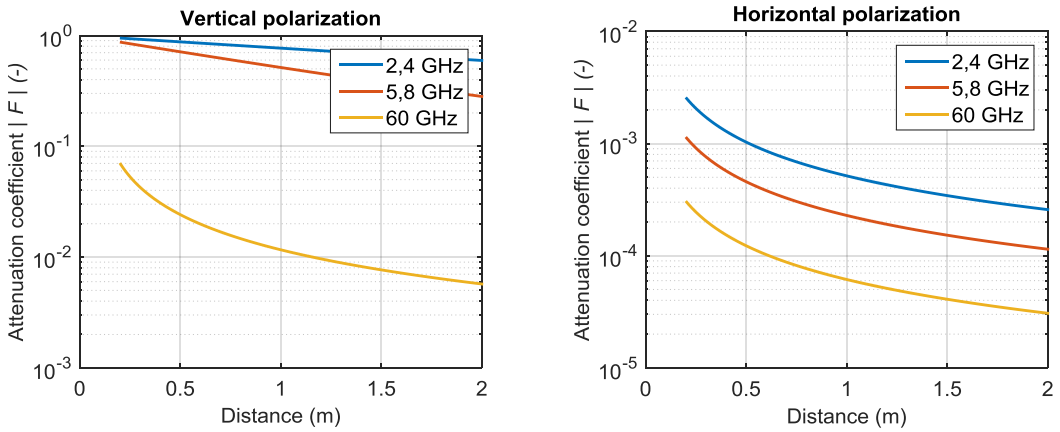

Figure 4.3: The dependence of the Sommerfeld attenuation coefficient on the distance between antennas for the vertical polarization (left) and the horizontal polarization (right).

The Sommerfeld attenuation coefficient for the vertical polarization is used to compute the electric field radiated by the vertical dipole on the surface of the metal plate. In this case, only the surface wave is propagating between the transmit antenna and the receive one $\mathbf{E}_{sur}$ [4.1]:

$$E_{sur} = j30kIdl\left[(1 + R_V)F\frac{e^{-jkR}}{R}\right] \tag{4.11}$$

Here, k is the free-space wave number, R_V is the Fresnel coefficient, R is the distance between the dipole and the observation point.

The transmission between the transmitter and the receiver (electromagnetic wave guided by the conductive surface) can be evaluated by

$$S_{21} = 20log\frac{E_1}{E_0} \tag{4.12}$$

Here, E_1 is electric field intensity in the receiving point and E_0 is the electric field intensity at the transmitting point.

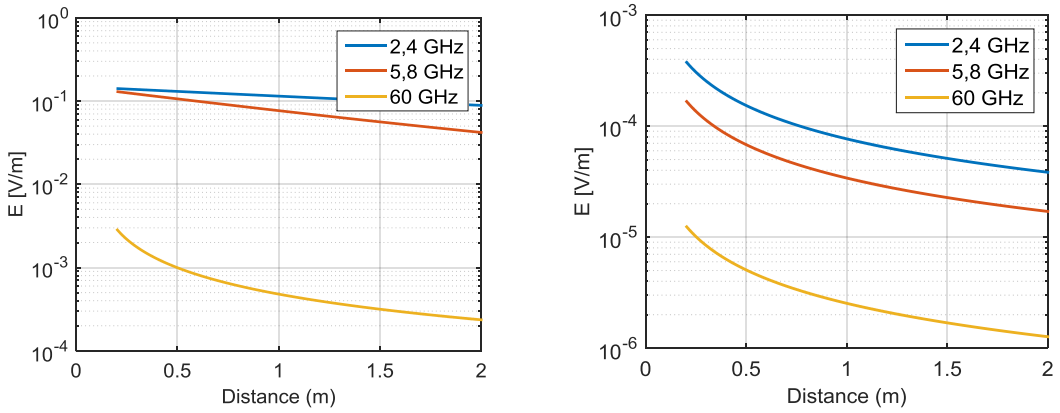

Figure 4.4: The dependence of electric field intensity on the distance between antennas for the vertical polarization (left) and the horizontal polarization (right).

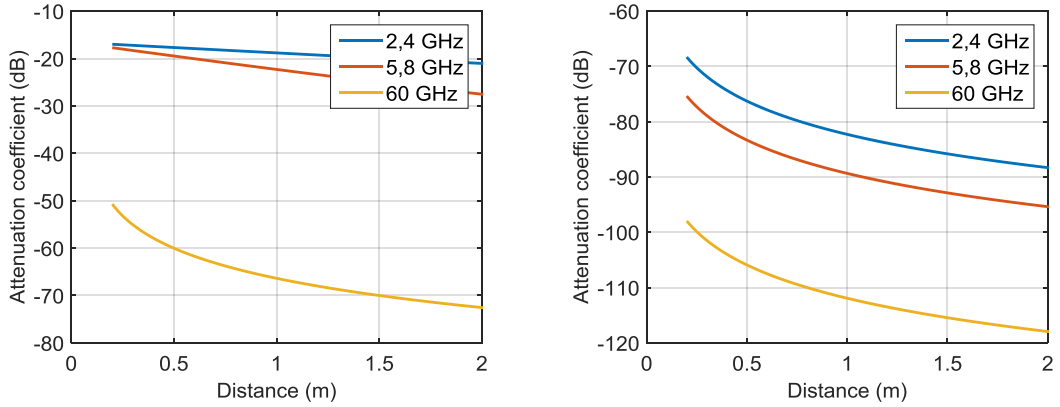

Figure 4.5: The dependence of the attenuation on the distance between antennas for the vertical polarization (left) and the horizontal polarization (right).

Considering dependences in Figures 4.3 to 4.5, only the vertical polarization will be considered due to the significantly lower attenuation.

The analytical model is compared with computations in CST Microwave Studio at frequencies 2.4 GHz and 5.8 GHz. Simulations differ by the excitation of surface waves:

- A waveguide port without waveguide; Figure 4.6;
- A monopole; Figure 4.7;
- An open-ended waveguide (Figure 4.8).

In each simulation, the transmission between the antennas was computed. The distance betwenn the antennas was changed from 0.20 m to 1.40 m with the step 0.02 m. Since the antennas considerably influence results, the transmission was normalized (Figures 4.9 to 4.11)

$$|E(r)| = |E_0| \frac{e^{-jkr}}{r} \tag{4.13}$$

Here, E(r) is electric field in the distance r from source, E_0 is electric field at source and $e^{-jkr} = 1$.

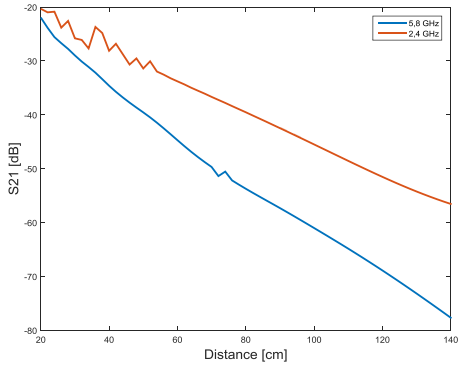

Figure 4.6: Waveguide port attenuation.

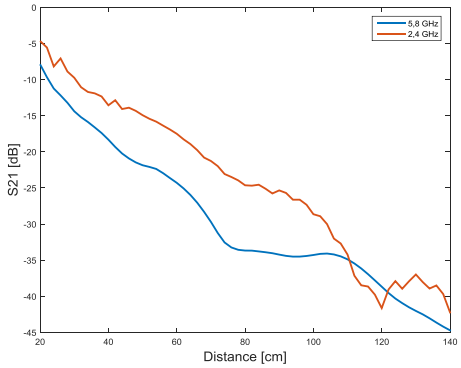

Figure 4.8: Open-ended waveguide

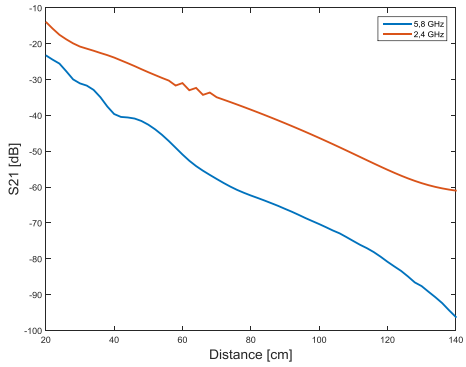

Figure 4.7: Monopole antenna attenuation.

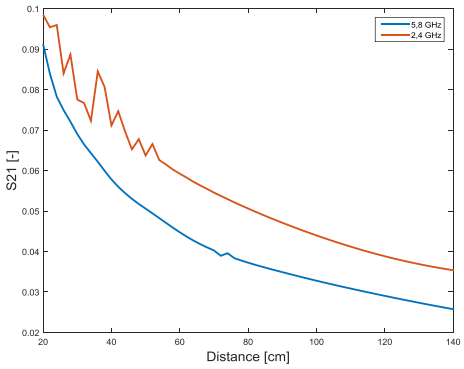

Figure 4.9: Normalized waveguide port attenuation.

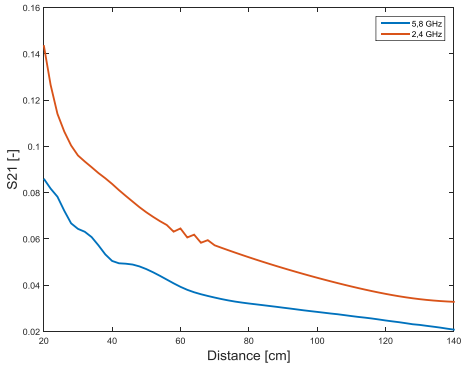

Figure 4.10: Normalized monopole antenna attenuation.

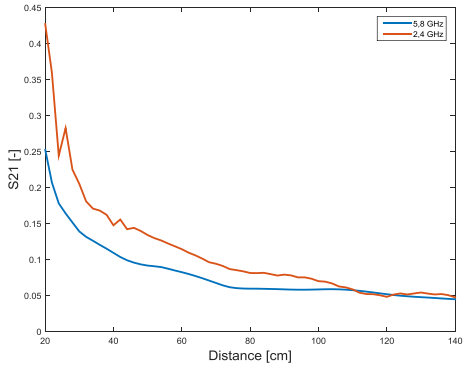

Figure 4.11: Normalized open-ended attenuation waveguide attenuation.

Finally, the transmission between antennas was measured (see the block diagram in Figure 4.12 and the measuring workplace in Figure 4.13). Using an antenna holder, 24 distances between antennas were set, and the transmission was measured (Figures 4.14 and 4.15).

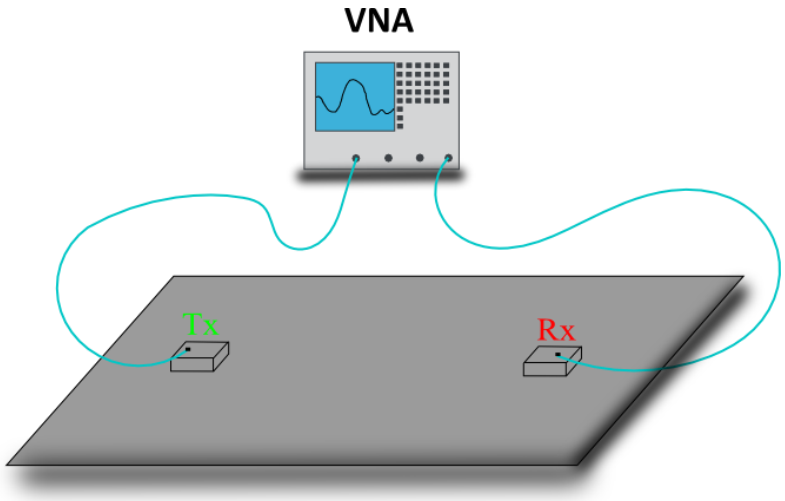

Figure 4.12: Illustrative block diagram of the measuring workplace.

Figure 4.13: The measuring workplace for monopoles (left) and waveguide (right)

The transmission S_{21} was measured by the vector network analyzer Rohde & Schwarz ZVL 13 in frequency bands 2.40 GHz to 2.50 GHz and 5.45 GHz to 5.75 GHz for deferent distances between antennas (Figures 4.14 and 4.15). The output power was set to 0 dBm and the resolution bandwidth was chosen as 100 Hz. For the bandwidths 100 MHz (ISM 2.4 GHz) and 300 MHz (ISM 5.8 GHz) and frequency steps 100 kHz (ISM 2.4 GHz) and 300 kHz (ISM 5.8 GHz), we measured 1001 frequency points. Used monopole antennas and open-ended waveguides were connected to the vectro network analyzer by phase stable coaxial cables.

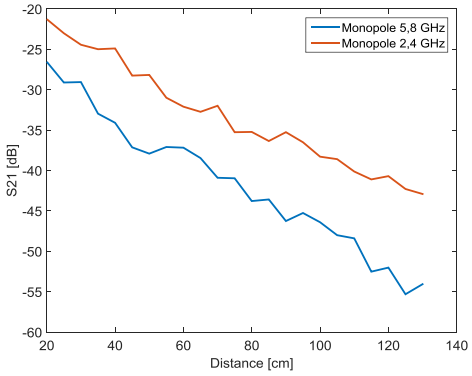

Figure 4.14: Transmission between antennas measured above the metal plate (monopole antenna).

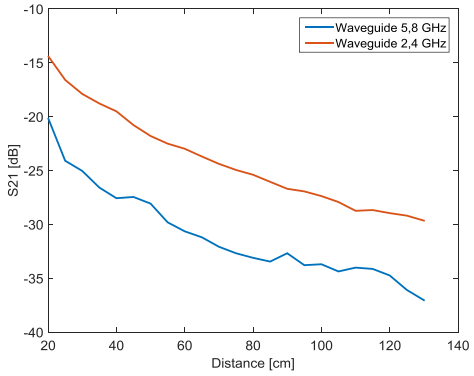

Figure 4.15: Transmission between antennas measured above the metal plate(open-ended waveguide)

The measured transmission is shown for two monopole antennas in Figures 4.14 and for two open-ended waveguides in Figure 4.15.

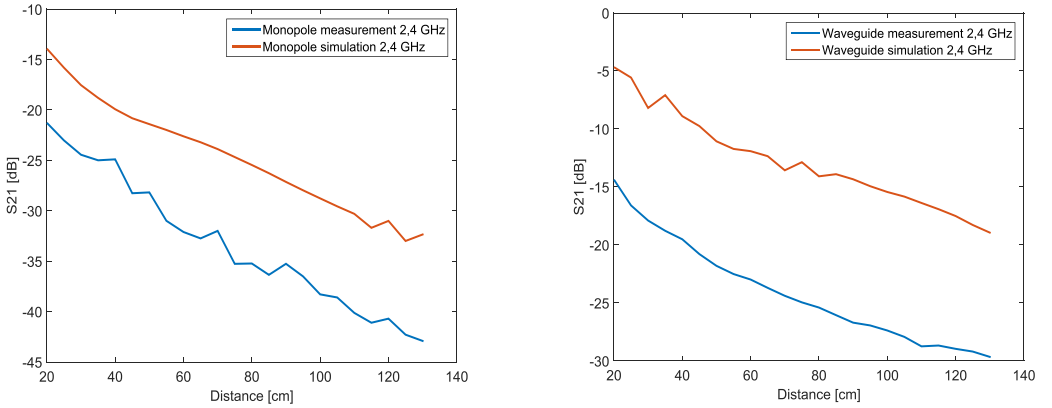

Figure 4.16: Comparison of the simulation and measurement of the transmission at 2.4 GHz for monopole antennas (left) and open-ended waveguides (right).

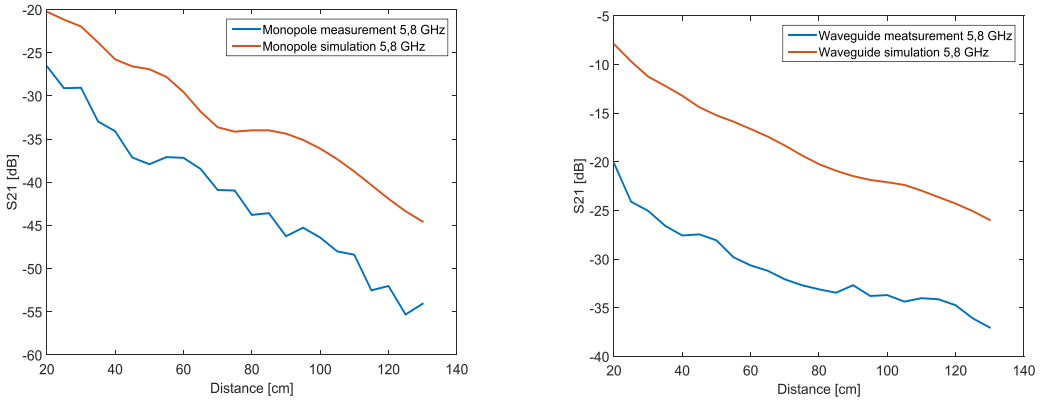

Figure 4.17: Comparison of the simulation and measurement of the transmission at 5.8 GHz for monopole antennas (left) and open-ended waveguides (right).

Figures 4.16 and 4.17 show the measured transmission for monopole antennas and open-ended waveguides. The open-ended waveguides exhibit the transmission higher for about 8 dB compared to the monopole antennas due to the higher directivity.

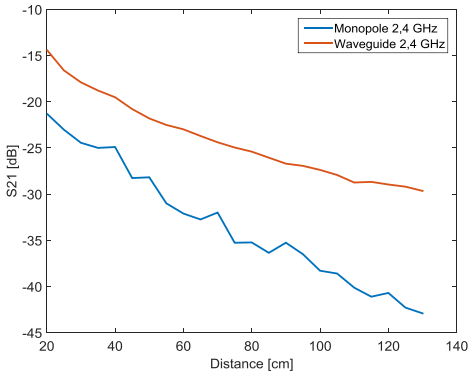

Figure 4.18: Transmission between antennas measured above the metal plate at 2.4 GHz (monopole versus open-ended waveguide).

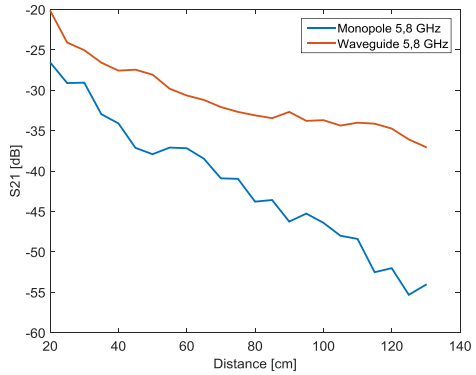

Figure 4.19: Transmission between antennas measured above the metal plate at 5.8 GHz (monopole versus open-ended waveguide)

Figures 4.18 and 4.19 directly compare the measured transmission between monopole and waveguide antennas at 2.4 GHz and 5.8 GHz. The figures show that the difference between the monopole and the open-ended waveguide increases with the distance between the antennas.

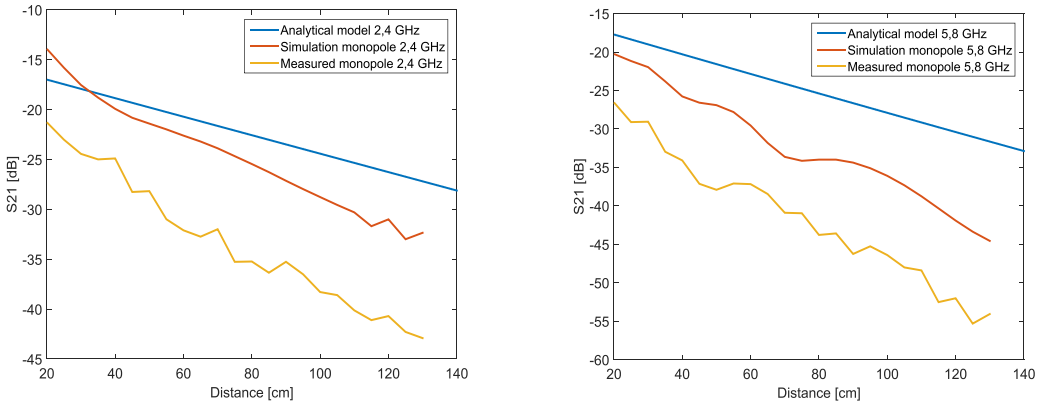

Figure 4.20: Comparison of the analytical model, simulation and measurement of the transmission between monopole antennas at 2.4 GHz (left) and 5.8 GHz (right).

The comparison of analytical models, simulations and measured values are shown in Figures 4.20 and 4.21. The measured dependency is corrugated by waves reflected in the laboratory. Nevertheless, the agreement among all the models and measured values is reasonable. Deferent absolute values od dependencies are caused by the different broadcasting power. Moreover, ideal objects without loses are considered in simulations.

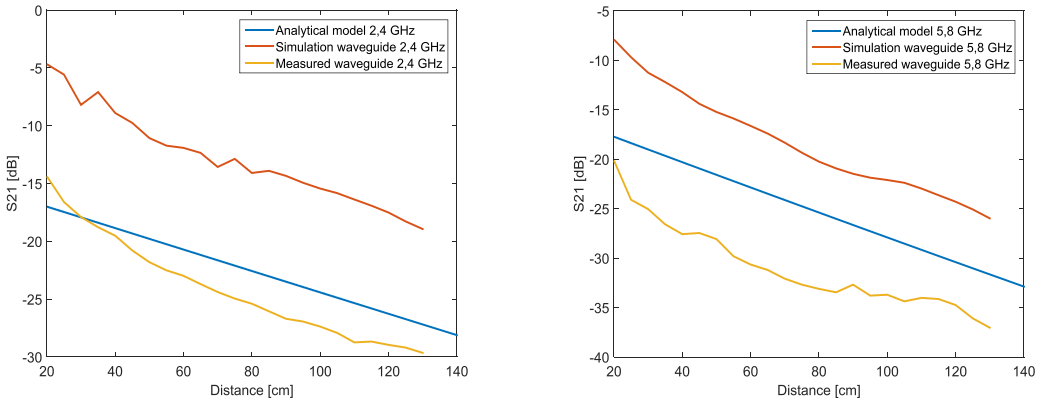

Figure 4.21: Comparison of the analytical model, simulation and measurement of the transmission between open-ended waveguides at 2.4 GHz (left) and 5.8 GHz (right).

The presented results show that the analytical model of a surface wave propagating along a metallic surface agrees with the numerical simulation in CST Microwave Studio and measurements, both for the monopole antenna and the open-ended waveguide, both in the ISM frequency band 2.4 GHz and 5.8 GHz. In the next step, the described experiments have been repeated inside a car (Figures 4.22 and 4.23).

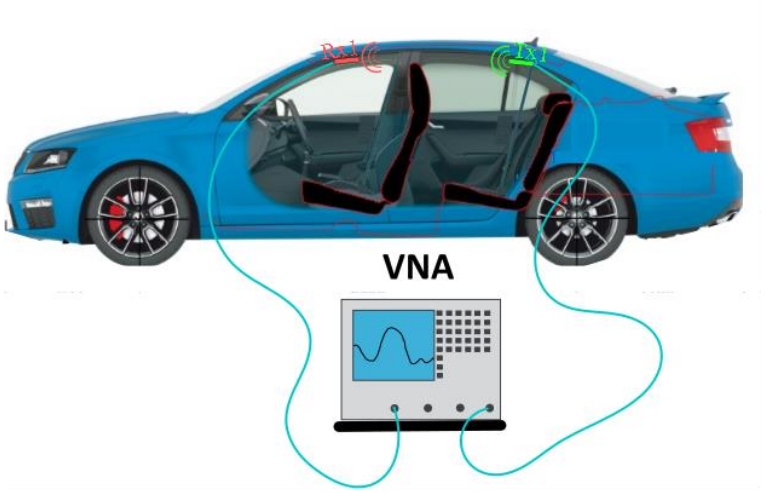

Figure 4.22: The block diagram of transmission measurements in a car: side view.

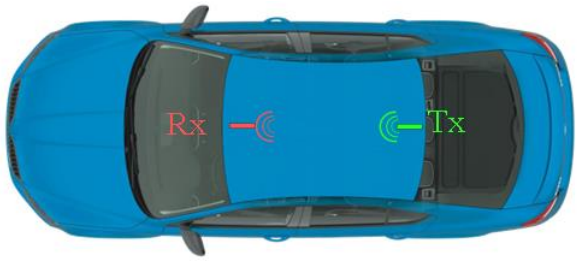

Figure 4.23: The block diagram of transmission measurements in a car: top view.

The measurements were carried out in a Skoda Octavia III 1.8 TSI Limousine. The surface wave was excited along the inner surface of a roof. All the measurement parameters and measuring antennas were identical with the laboratory measurement of surface waves propagating along the metal plate to ensure the same measurement conditions.

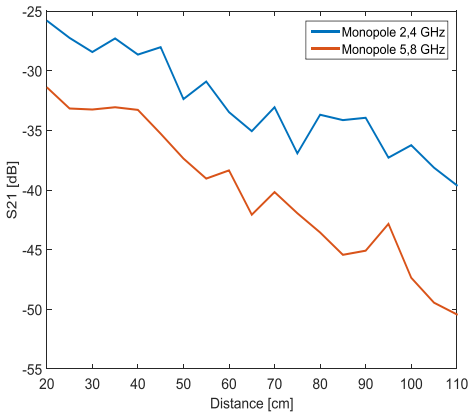

Figure 4.24: Measured transmission between monopole antennas above the car roof.

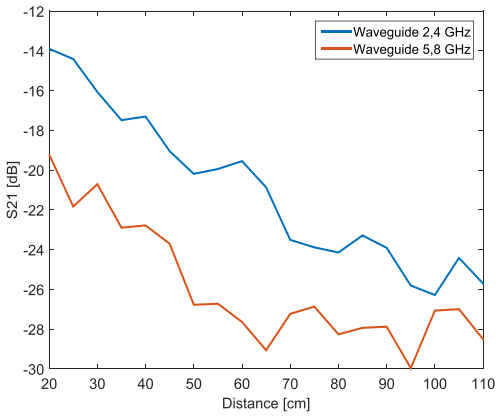

Figure 4.25: Transmission between antennas measured above the car roof at 2.4 GHz monopole versus open-ended waveguide).

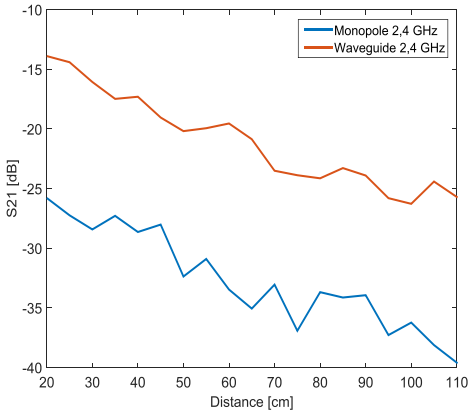

Figure 4.26: Measured transmission between open-ended waveguides above the car roof.

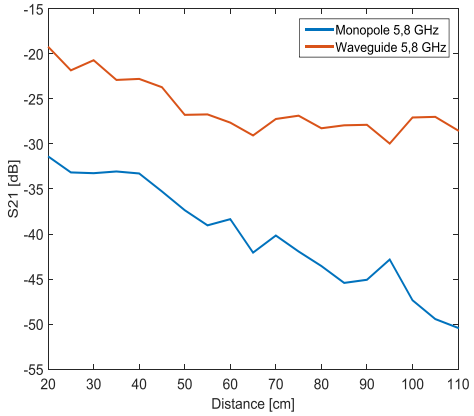

Figure 4.27: Transmission between antennas measured above the car roof at 5.8 GHz (monopole versus open-ended waveguide).

Figures 4.24 and 4.25 show transmissions measured in the car depending on a distance between antennas. Compared to the analytical models or laboratory measurements, the measured dependences are not smooth because the car is a complex environment supporting a multi-path propagation of electromagnetic waves. Due to the multi-path propagation, different field-intensity values are measured for different distances between the antennas. The distances varied from 20 cm to 110 cm (physical dimensions of the car did not allow measuring the distance longer than 110 cm).

The transmission measured between the monopole antennas (Figure 4.24) shows that the transmission is higher for 4 dB at 2.4 GHz, approximately. The difference is even higher for open-ended waveguides (Figure 4.25) due to a higher directivity of the waveguide antenna. The measured values correspond with analytical results and simulation models (see Figures 4.28 and 4.29).

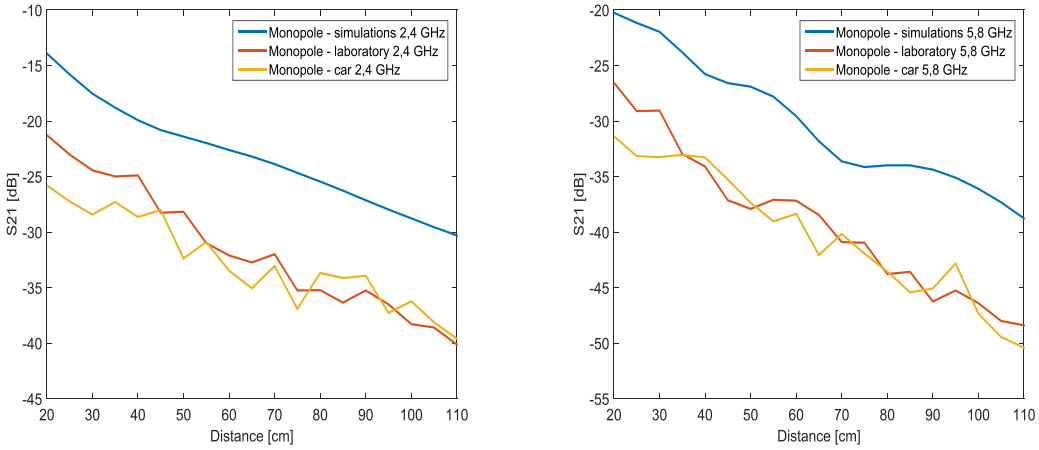

Figure 4.28: Comparison of the transmission between monopole antennas at 2.4 GHz (left) and 5.8 GHz (right): simulation versus measurements in a car and above the metallic plane.

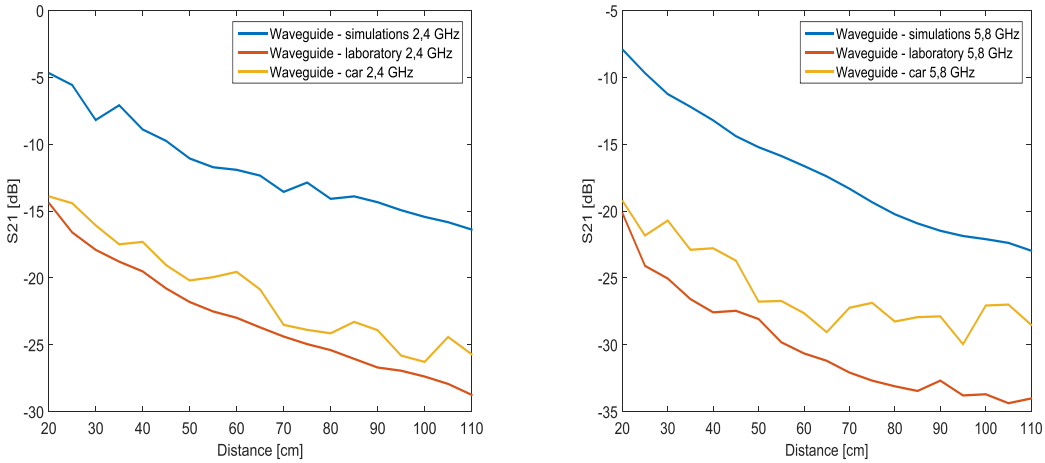

Figure 4.29: Comparison of the transmission between open-ended waveguides at 2.4 GHz (left) and 5.8 GHz (right): simulation versus measurements in a car and above the metallic plane.

4.2 Conclusions

Considering results of analytical, numerical and experimental characterization of wireless transmission channels in cars, which were presented in this chapter, we can define a sequence of steps forming the methodology of the characterization:

1. Analytical description of surface waves propagating along the conductive surface of the car. Surface waves can be approximated in terms of Norton waves propagating above a conductive surface. This analytical approach brings an efficient a quick characterization of a wireless channel.

2. Numerical simulation of surface waves. Wave propagation above a conductive surface can be simulated numerically using realistic antennas. Comparison of the numerical simulation and analytical computations allows us to calibrate sources to obtain corresponding results.

3. Simplified laboratory measurements. Wireless transmission channel can be built in a laboratory using real antennas above a conductive surface. Using a proper configuration of the experiment and a proper calibration, reflections can be minimized, and a good agreement with analytical and numerical models can be obtained. That way, the measuring system can be properly set for measurements in a real car.

4. Measurements in real cars.

Performing the described steps, reliable training patterns can be composed for training artificial neural models as described in the next chapter.

Trained neural networks play the role of black-box models of electromagnetic environment in a car. These models can be used for approximate CPU-time efficient and memory-moderate computer simulations of in-car wireless communication.

4.3 References

[4.1] E. C. Jordan and K. G. Balmain, *Electromagnetic Waves and Radiating Systems*, 2/E, Prentice Hall: Englewood Cliffs, 1968.

[4.2] M. Kotol and Z. Raida, Models of wave propagation along car roof, *Radioelektronika 2017*, Brno, p. 100-104, ISBN: 978-1-5090-4594-5.

Chapter 5

Neural modeling of in-car wireless channels

In this chapter, we describe modeling of a CTF between antennas placed inside a car. The transmission considers a relative position of antennas. Transmission channels can follow the surface of a metallic body of a car (chapter 5.1), or can be created inside the car (chapter 5.2). Since parameters of the channels are influenced by passengers inside the car, variations of CTF can be used for the estimation of the occupation of seats (chapters 5.3 and 5.4).

5.1 Channel along car body at 60 GHz

The experimental research was focused on a wireless power transfer along an inner surface of a vehicle. Thanks to such a concept, the amount of the necessary cabling can be reduced. For the described service, we have selected the 60 GHz ISM band. A high attenuation in this band provides a spatial isolation for personal area networks (PAN) and wireless local area networks (WLAN) [5.1]. PAN and WLAN can be advantageously used for in-vehicle communication.

Numerical modeling of wireless in-car communication is extremely time-consuming at 60 GHz due to electrically large dimensions of in-car objects. Therefore, we have proposed an artificial neural network (ANN) to be used for efficient modeling. Attention is turned to feed-forward (FF) networks and radial basis function (RBF) networks.

The transmission between the transmit antenna and the receive antenna at different positions in a car was measured in the frequency band from 60 GHz to 62 GHz. Antennas were placed on the inner surface of the roof, and the transmission along the roof was measured depending on the location of the transmit antenna and the receive antenna. The transmit antenna was placed at a position Tx1 and the receive antenna was located at the position Rx1.

We successively changed the position of the receive antenna Rx2 and Rx3, and the position of the transmit antenna Tx2 and Tx3. The transmit antenna was placed under the right rear pillar, the left rear pillar and the back center. The receive antenna was placed under the right front pillar, the left front pillar and the front center. Schematics of location of the antennas are shown in Figure 5.1.

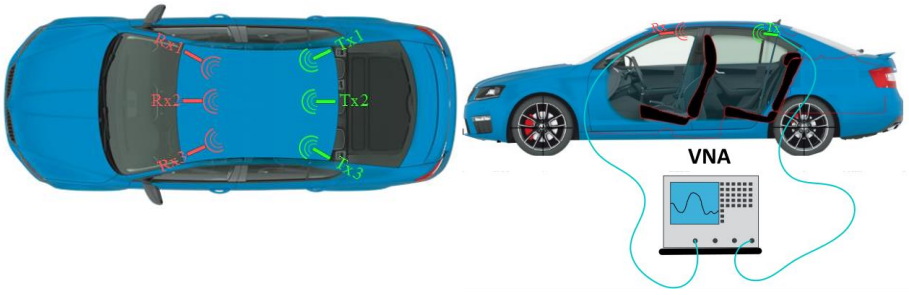

Figure 5.1: Location of 60 GHz antennas.

For each TX – RX configuration, we measured the transmission coefficient S_{21} in 60 GHz ISM band by the vector network analyzer (VNA) Rohde & Schwarz ZVA 67. The output power was set to 0 dBm and the resolution bandwidth used for all measurements was 100 Hz. We set the bandwidth of measurement to 2 GHz. The frequency step was 10 MHz which provided 201 measured frequency samples. As an antenna, we used the open end of the waveguide WR 15. The waveguide was connected to the VNA by a phase stable coaxial cable. The measurement was carried out in Skoda Octavia III 1.8 TSI Limousine.

In a car, we measured the CTF in the frequency range from 60 GHz to 62 GHz with frequency step of 10 MHz for various positions of the transmit antenna and the receive antenna. In order to illustrate measurement and modeling results, we have chosen the position of the transmit antenna Tx2 and the positions of the receive antenna Rx1, Rx2, and Rx3 for explanations.

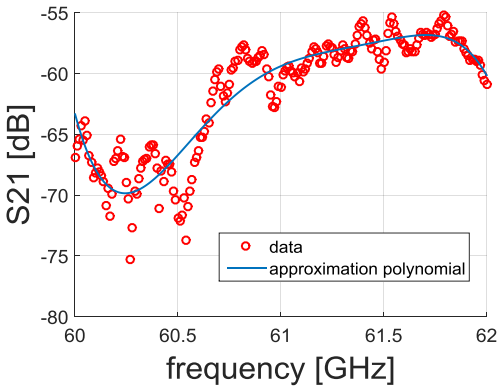

Figure 5.2: Measured frequency response of the CTF between the transmit antenna Tx2 and the receive antenna Rx1 (red). Polynomial approximation of frequency response (blue).

Figure 5.2 shows measured frequency response of the CTF between the transmit antenna Tx2 and the receive antenna Rx1 (red circles). The measured data were approximated by a low-order polynomial to obtain a smooth-enough function for training NN (blue line). Such a way, CTF of all the measured Tx – Rx combinations were processed.

In order to train the ANN, proper input patterns [frequency, position of transmit antenna, position of receive antenna] and output targets [magnitude of transmission coefficient] have to be composed. The training frequency was changed from 60 GHz to 62 GHz with the frequency step 150 MHz. All the combinations of Tx antenna positions and Rx antenna positions were considered.

The models were created using radial basis function (RBF) network and the feed-forward (FF) network. During training, the input patterns were introduced to the input of the ANN, and weights were changed to obtain corresponding output targets at the output of the ANN. The training process was stopped when the relative training error reached 10^{-6} which was selected from previous experiences. Further parameters for stopping training were the number of training cycles (55 for RBF ANN and 1000 for FF ANN).

In Figure 5.3, the configuration of RBF ANN used for the estimation of the transmission coefficient between antennas is shown. Symbols x_1 to x_n denote input signals, w_{11} to w_{nm} are synoptic weights of neurons, and f_1 is an output signal.

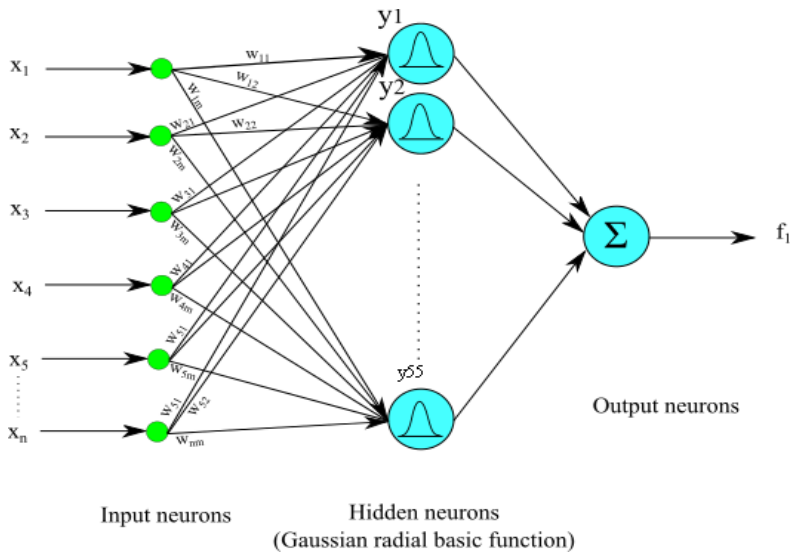

Figure 5.3:RBF network for approximating 60 GHz channel along the roof of a car.

The FF ANN contained three hidden layers with 15 neurons in the first layer, 7 neurons in the second layer and 15 neurons in the last layer. And all the hidden neurons had the bipolar sigmoidal activation function.

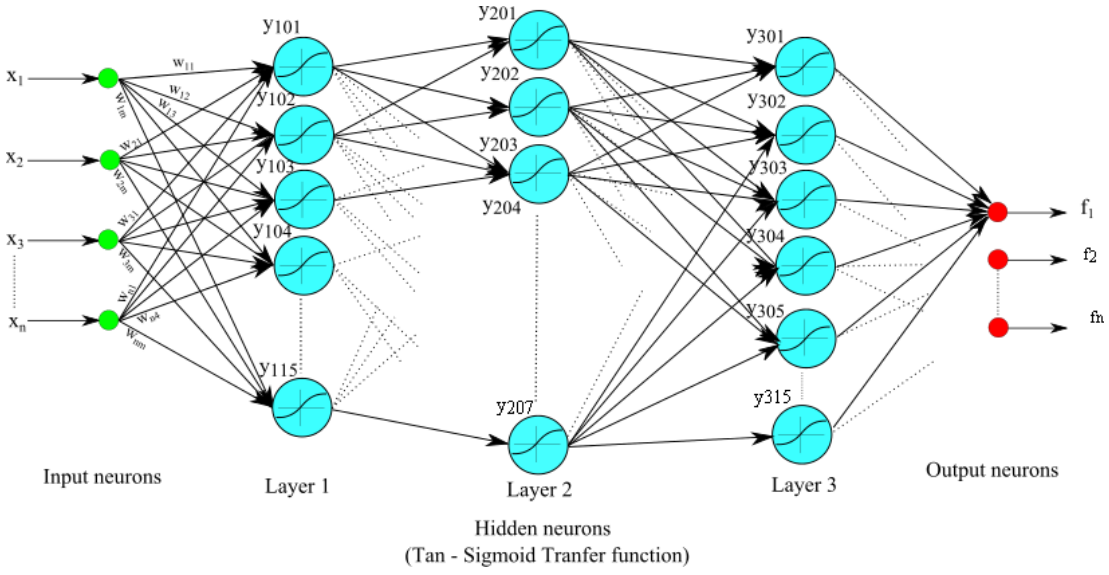

Figure 5.4:FF network for approximating 60 GHz channel along the roof of a car.

In Figure 5.4, the configuration of ANN used for the estimation of the transmission coefficient between antennas is shown. Symbols x_1 to x_n denote input signals, w_{11} to w_{nm} are synoptic weights of neurons, and f_1 is an output signal.

In the next step, the trained ANN has to be verified. For the verification, we have to use input patterns which differ from training ones. In our testing, different frequencies were used.

The results of the estimation of the CTF between the transmit antenna and the receive antenna at testing frequencies for FF ANN are shown in Figures 5.5 to 5.7. Red circles represent measured values of the CTF, and the blue line corresponds to estimated values of the CTF. Obviously, FF ANN estimates the CTF with a good accuracy. Figure 5.11 shows the relative estimation error of the FF ANN.

The RBF ANN results of the estimation of the CTF between the transmit antenna and the receive antenna are shown in Figures 5.8 to 5.10. Figure 5.12 shows that the error of RBF estimates is similar for all three antenna configurations.

Using outputs of practical measurements, training sets for both the FF network and the RBF network were prepared. Networks were trained to estimate the CTF between the transmit antenna and the receive antenna depending on the location of antennas and the operation frequency from the band 60 GHz to 62 GHz. Functionality of neural models was verified on testing patterns which differ from training ones by the frequency. The estimation error does not exceed the level of 4 per cent (see Figures 5.11 and 5.12).

5.2 Channel inside car in UWB frequency band

In the following text we describe characteristics of the CTF inside the car. These characteristics are very important for future in-car communication technologies. Future technologies will create the small wireless networks for the distribution of data services such as internet, video, audio, etc. For these services, we prefer to use the UWB frequency band from 3 GHz to 11 GHz because of the hardware support availability. An estimation of CTF characteristics is a time-consuming and computationally demanding process.

Let us turn the attention to the channel transfer function estimation for different receiving antenna locations determined by a two-dimensional grid using ANN. The proposed ANN can be based on the FF and RBF ANN. The ANN has been optimized using measured channel transfer function to achieve better effectiveness, speed and accuracy.

The reliable communication and high efficient low energy transfer inside the vehicles are considered to be prospective technologies for future applications in automotive industry. Many companies have started to deploy modern wireless networks in cars for increasing traveling comfort. In order to apply such technologies in future cars, the detailed knowledge of the CTF is necessary. The communication band from 3 GHz to 11 GHz seems to be very prospective.

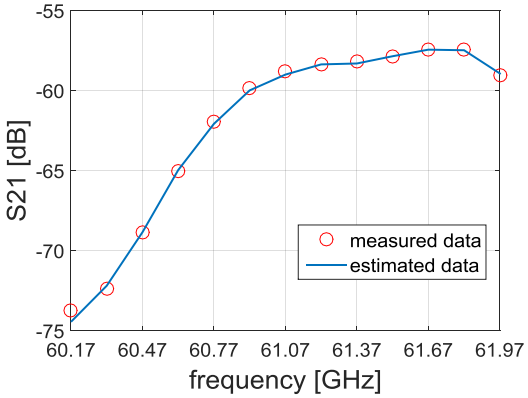

Figure 5.5: Frequency response of CTF between Tx2 and Rx1. Measured (red) versus FF ANN estimated (blue).

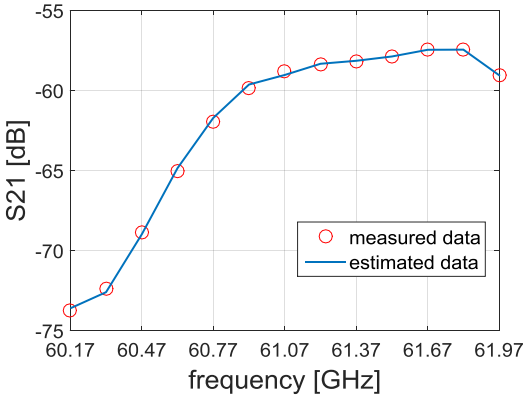

Figure 5.8: Frequency response of CTF between Tx2 and Rx1. Measured (red) versus RBF ANN estimated (blue).

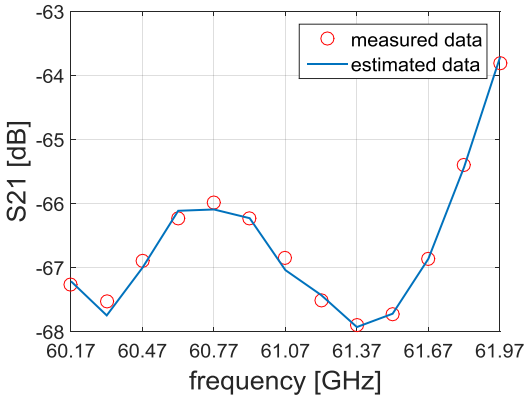

Figure 5.6: Frequency response of CTF between Tx2 and Rx2. Measured (red) versus FF ANN estimated (blue).

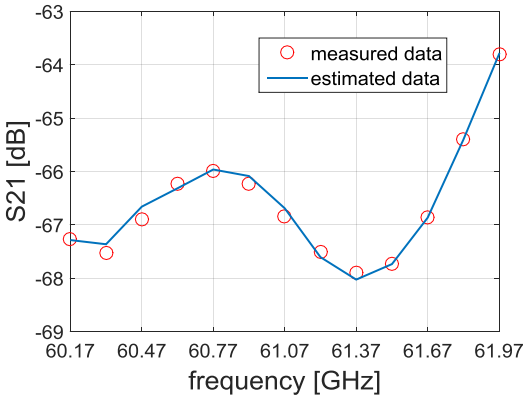

Figure 5.9: Frequency response of CTF between Tx2 and Rx2. Measured (red) versus RBFANN estimated (blue).

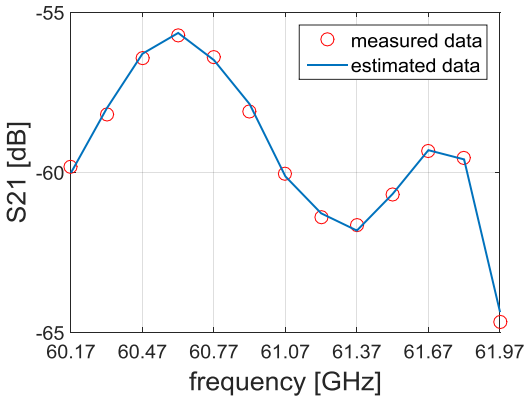

Figure 5.7: Frequency response of CTF between Tx2 and Rx3. Measured (red) versus FF ANN estimated (blue).

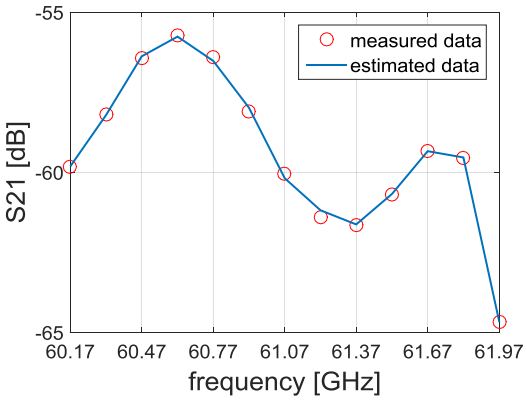

Figure 5.10: Frequency response of CTF between Tx2 and Rx3. Measured (red) versus RBFANN estimated (blue).

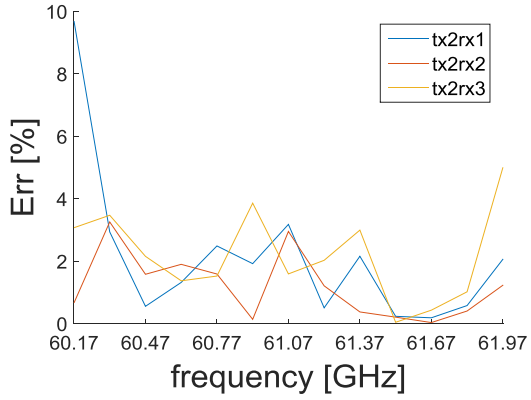

Figure 5.11: Relative error of FF ANN estimation of the CTF between antennas.

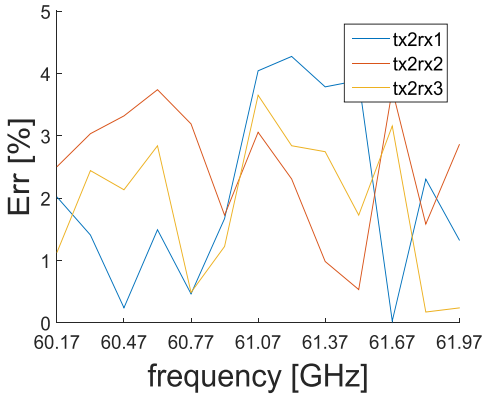

Figure 5.12: Relative error of RBF ANN estimation of the CTF between antennas.

However, the signal propagation in the car comprises many physical phenomena due to the composition and configuration of the interior (ceiling, windows, seat, body, luggage, persons…) In [5.2], several approaches to modeling the inner channel are shown.

The paper [5.3] presents the ultra-wideband (UWB) channel measurement and modeling for an intra-vehicle environment. Measurement and processing according to the position transmitting and receiving antennas in car was investigated in [5.4]. The simple but robust model characterizing the frequency dependent transfer function of an in-vehicle UWB channel was presented in [5.5]. We have proposed another approach to modeling the channel in the car, based on RBF ANN and FF ANN.

Figure 5.13: Location of UWB antennas.

In order to provide the in-car channel transfer function (CTF) estimation, the transmission characteristics between antennas were thoroughly measured. Mutual TX – RX antenna positions were obtained using the antenna polystyrene holder offering one hundred possible RX antenna locations in the grid of 3 × 3 cm (see Figure 5.13). For each TX – RX configuration, the CTF was measured. The CTF corresponding to S_{21} were measured by the four port vector network analyzer (VNA) Agilent Technologies E5071C. The output power was set to 5 dBm and the

resolution bandwidth used for all measurements was chosen as 100 Hz. We set the bandwidth 8 GHz. The frequency step 10 MHz provided 801 measured frequency points. We used monocone antennas, which were connected to the VNA by phase stable coaxial cables. The measurement was carried out in a Skoda Octavia III 1.8 TSI Limousine.

The TX antenna was located in the front left corner of the car and the grid for the receiving antenna was placed into the rear right seat. In Figure 5.14, both the TX and RX antennas are depicted in the measuring locations.

Figure 5.14: UWB measurements in a car.
Left: the receive antenna, right: the transmit antenna.

The antenna holder with the grid for the RX antenna is located on the right back seat. This location was chosen to correspond to positions of communication devices (mobile phone, tablet, etc.). Positions can be changed with the increments of 3 cm.

For the NN training, the coordinates (creating the NN input patterns) of only each fifth location (increment 15 cm) was used, which gives 20 training patterns and corresponding CTF patterns (NN output patterns) were used. The training process was stopped when the relative training error lower than 10^{-6} was reached or the maximum number of iterations was performed (100 for RBF ANN or 600 for FF ANN). To evaluate the trained ANN robustness and accuracy of CTF estimation, we created a number of new input patterns formed by previously unused coordinates.

The configuration of RBF ANN used for the estimation of the transmission between antennas is identical with the structure depicted in Figure 5.3. On the contrary, the FF ANN contains two hidden layers with 130 neurons in the first layer and 15 neurons in the second layer. All the hidden neurons have the bipolar sigmoidal activation function (see Figure 5.15). Here, symbols x_1 to x_n denote input signals, w_{11} to w_{nm} are synoptic weights of neurons, and the rest of symbols denote output signals.

Training started with randomly set synoptic weights for all ANN. Training of the RBF ANN took 30 seconds and training the FF ANN took 75 seconds. The training time depends on the computational power of PC.

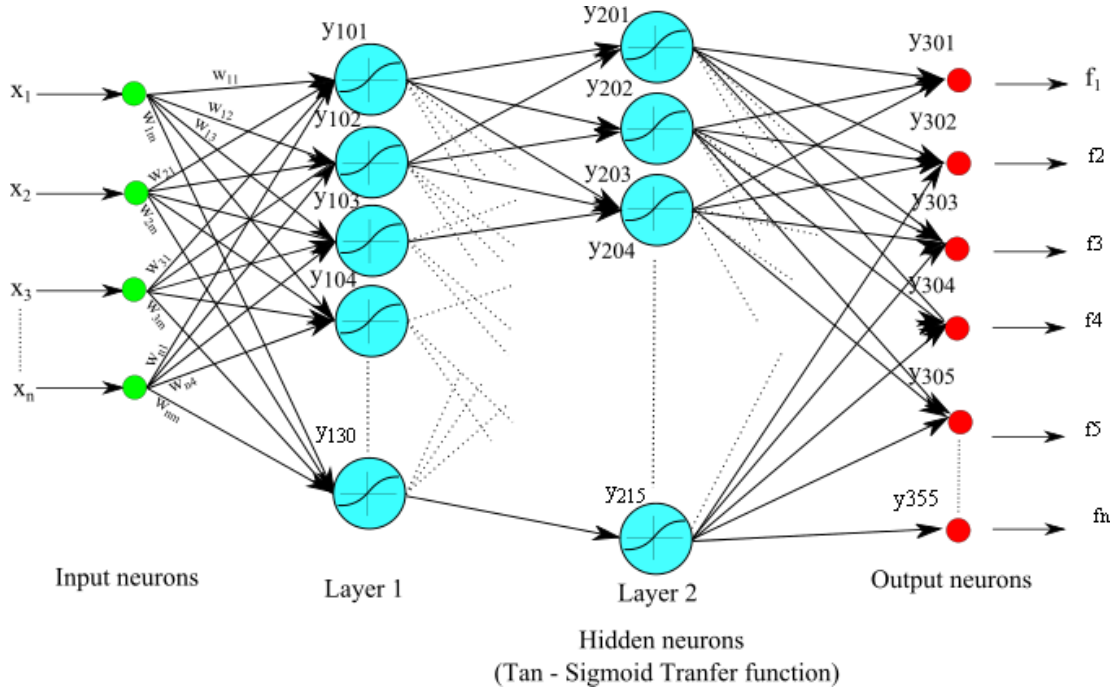

Figure 5.15: FF network for approximating UWB channel inside a car.

The results of the CTF estimation between the TX and RX antennas for FF ANN are shown in Figures 5.16 and 5.17. Red points represent measured values approximated by a polynomial function of the CTF, and the blue line represents the estimated values of the CTF. The RBF ANN results of the estimation of CTF between the TX and RX antennas are shown in Figures 5.19 and 5.20. Figures 5.18 and 5.21 can show the relative estimation error of the NN.

5.3 Neural estimator of passengers at 60 GHz

A neural estimator of seats occupied by passengers in a vehicle is introduced in this chapter. The estimator is built from the RBF NN. Occupied seats in a vehicle are estimated from CTF between antennas operating in 60 GHz ISM band. The passengers and their localization have an influence on the shape of the transmission function.

Localization of people or machines is used indoor often. Existing wireless localization is infrared, ultrasonic or radio-frequency one. The infrared technology requires a direct line of sight and can be used for short distances only. The ultrasonic localization requires building the infrastructure in the transmission or reception of the system [5.6].

Radio Frequency Identification (RFID) is low cost. However, this system requires the construction of a large infrastructure to provide seamless localization and identification. Using RFID in a large scale can be difficult m [5.6]. Each localized object must have a tag.

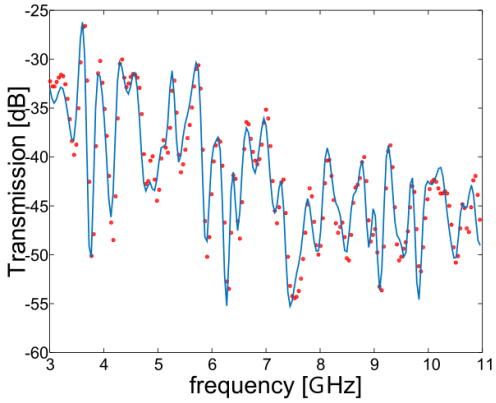

Figure 5.16: Frequency response of CTF between Tx and Rx (position 1). Measured (red) versus FF ANN estimated (blue).

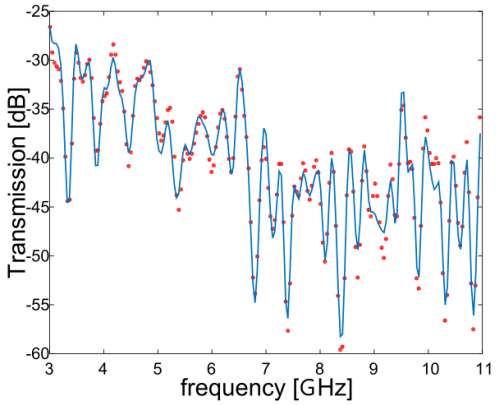

Figure 5.17: Frequency response of CTF between Tx and Rx (position 8). Measured (red) versus FF ANN estimated (blue).

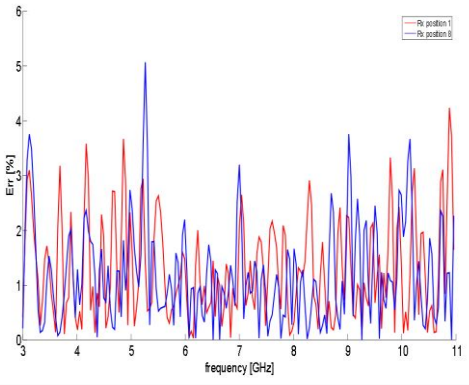

Figure 5.18: Relative error of FF ANN estimation of the CTF between antennas.

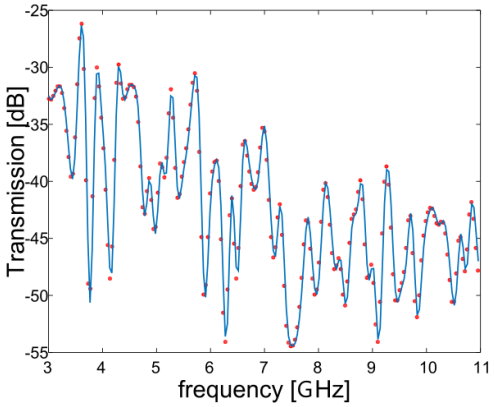

Figure 5.19: Frequency response of CTF between Tx and Rx (position 1). Measured (red) versus RBF ANN estimated (blue).

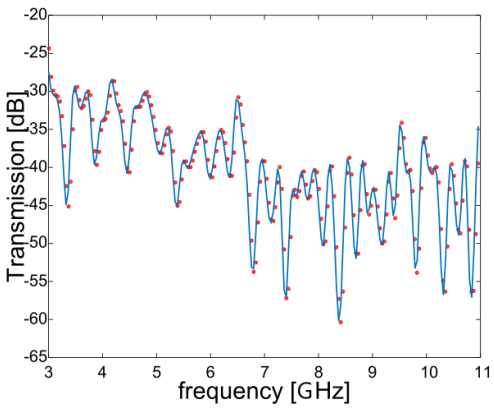

Figure5.20: Frequency response of CTF between Tx and Rx (position 8). Measured (red) versus RBF ANN estimated (blue).

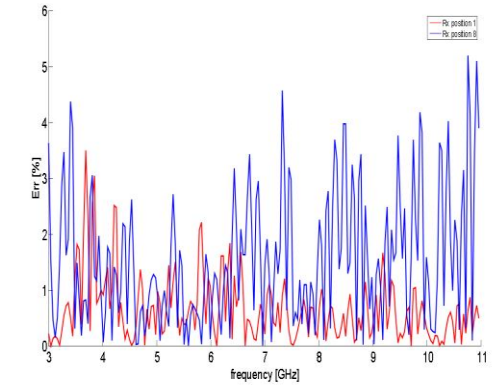

Figure 5.21: Relative error of RBF ANN estimation of the CTF between antennas.

.

For all configurations of passengers in a car and two TX – RX configurations (see Figure 5.22), we measured the CTF corresponding to S21. CTF parameters were measured in the 60 GHz ISM band by the port vector network analyzer (VNA) Rohde & Schwarz ZVA 67. The output power was set to 0 dBm and the resolution bandwidth used for all measurements was chosen as 100 Hz. We set the bandwidth to 10 GHz. The frequency step of 10 MHz provided 1001 measured frequency samples. We used an open end of the waveguide WR 15 as antennas. Waveguides were connected to the VNA by phase stable coaxial cables. The measurement was carried out in a Skoda Octavia III 1.8 TSI Limousine.

Figure 5.22: Location of 60 GHz antennas for localization.

The CTF between red antennas and green ones (Figure 5.22) were measured for all the possible configurations of passengers in a car. Each configuration was measured five times to suppress random variations caused by movement of persons in the car.

Outputs of described measurements CTF were used to train an ANN. The trained ANN was exploited to estimate occupied seats from measurements of CTF in a different car occupied by different passengers sitting in slightly shifted positions (to demonstrate robustness of the trained neural estimator).

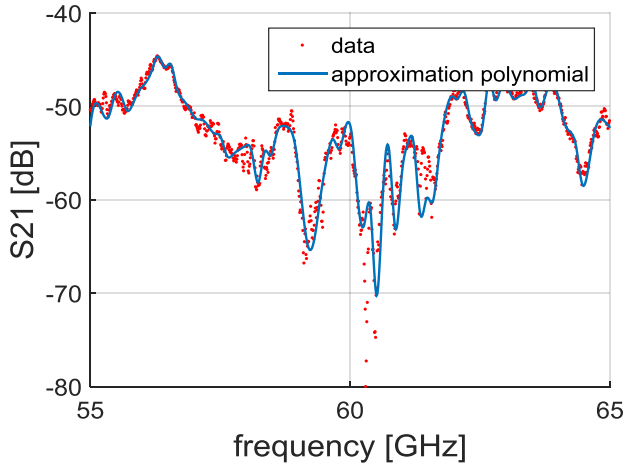

Figure 5.23: Measured frequency response of CTF between the antennas (red). Polynomial approximation of frequency response (blue).

Figure 5.23 shows measured values of the CTF between the Tx1 and the Rx1 (red points). Measured values were processed in Matlab, and ANN was implemented using Neural Network Toolbox of Matlab. The measured values were approximated by a polynomial function to partially smooth data for training NN (blue line). Smoothing of the measured data is equivalent to a low-pass filtering.

As an input training pattern, we created a matrix of operational frequencies and corresponding CTF coefficients for all the measured configurations of passengers.

From measured values, we created training patterns by selecting each 15^{th} value. Hence, training patterns were created by values with the frequency step 150 MHz. This approach was used for all the measured configurations.

The training sets were created from measured values as follows:

- As an input training pattern, we used a matrix of operational frequencies and corresponding CTF coefficients S21.
- As an output training pattern, we used a matrix of corresponding configurations of passengers.

All the configurations of passengers were considered. The training process was stopped when reaching the relative training error lower than 10^{-6}. Geometry of the used RBF ANN is identical with the structure given in Figure 5.3.

For verification of the trained ANN, we created a new input matrix. From values, which were measured in the band 55 GHz to 65 GHz with the step 10 MHz, we have randomly selected the starting sample between 2 and 14 (1 was used for training and 15 starts the following period). The rest of the sequence was formed from each 15^{th} sample from the starting one. That way, the verification matrix with the frequency step 150 MHz (different from the training one) was created.

The new input pattern (created by the described way) was introduced to the input of the trained ANN and the NN estimated configurations of passengers in the car. This estimation was compared with real configurations of persons. In order to demonstrate robustness of the trained ANN, CTF between antennas were measured for different passengers (small, tall, male, female) sitting in different cars in different positions (on seats, between two seats).

Configurations of persons in the car were numbered for better understanding. For example, the configuration #1 corresponds to a fully occupied car, and configuration #22 is the car with a driver only.

For illustration, Figures 5.24 and 5.26 show a selected training configuration (yellow circles indicate occupied positions) and a corresponding testing one (green circles indicate correct estimates of occupied positions and the red circle the wrong one).

Figure 5.25 shows the number of incorrect estimations for all standard configurations of passengers (the number of configuration follows the horizontal axis). In this case, we use the

same measurements for training and testing, but testing is done at different frequencies (as described above).

Figure 5.27 shows the number of incorrect estimations for all non-standard configurations of passengers (the number of configuration follows the horizontal axis). In this case, ANN was trained under standard conditions and tested on non-standard configurations. Obviously, non-standard configurations increase error rate of the estimator. Therefore, robustness of the ANN has to be improved by further development.

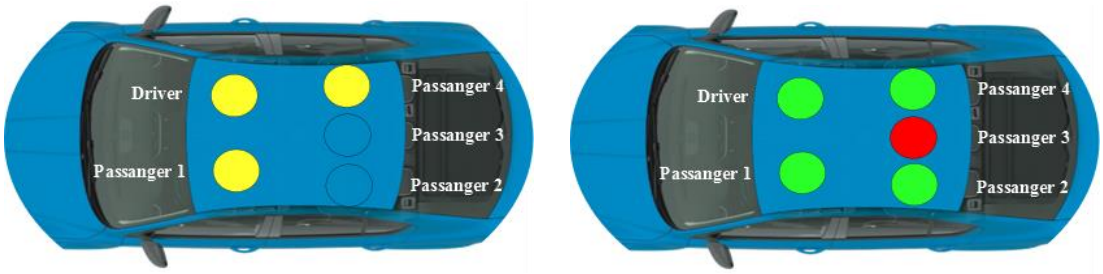

Figure 5.24: Configuration no. 9. Yellow: occupied,
green: correct identification, red: wrong estimation.

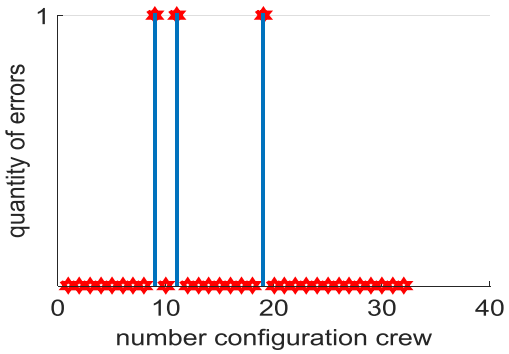

Figure 5.25: The number of wrong estimations
for 32 standard configurations of passengers.

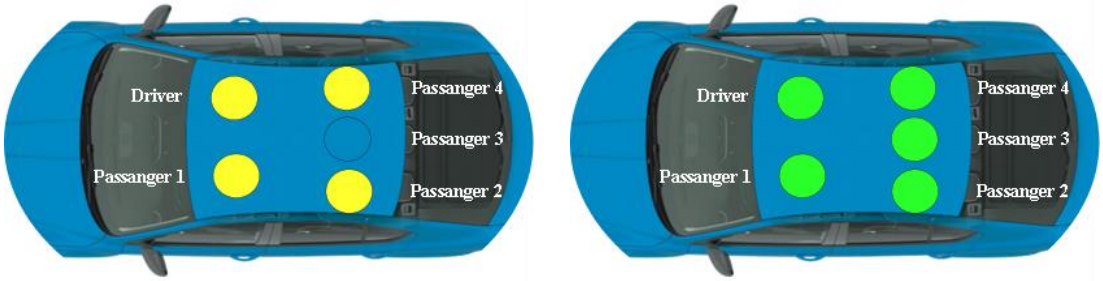

Figure 5.26: Configuration no. 4. Yellow: occupied,
green: correct identification, red: wrong estimation.

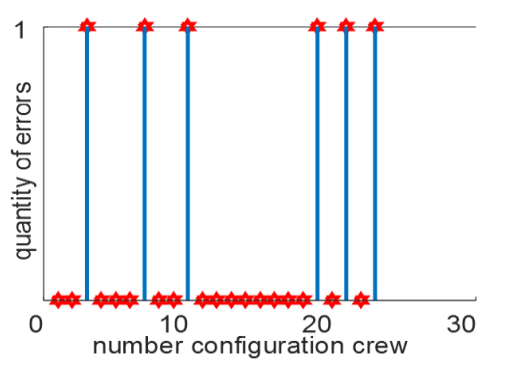

Figure 5.27: The number of wrong estimations
for 25 non-standard configurations of passengers.

A neural estimator of passengers in a vehicle was introduced. The estimator used ANN based on RBFs. For the ANN, we created an input training pattern and an output testing target. From measured frequency responses of CTF between the transmit antenna and the receive antenna, the neural estimator identified the corresponding configuration of passengers in a car.

Next, we measured non-standard configurations of passengers for the verification of robustness of the trained ANN: measured frequency responses of CTF were inserted to the input of the trained ANN and obtained responses were compared with real presence of passengers in the car.

5.4 Neural localization of passengers in UWB

The localization of a person by an artificial neural network applied on a measured CTF between antennas is discussed. Such localization can be useful in the case when we need a space protected against illegal entry or abandonment. The CTF affected by the person(s) contains information not only about the presence of people in the monitored area but also about their positions. The localization of people is discussed for small spaces. For this case, localization of passengers in a car was selected as an example of locating people. For localization, two types of neural architectures are used – the feed-forward and the radial basis function. CTF was measured at ultra-wideband frequencies (3 to 11 GHz). Each configuration of people was measured five times to suppress the movement effect. Training and verification patterns were composed of approximated CTFs by the least square fitting. Localization results are discussed in terms of estimation accuracy. According to our best acknowledge nobody is investigating this topic.

There are many ways of determining the location of objects. These techniques are dominantly based on:

- The radar principle – Electromagnetic pulses reflected from an object allow us to determine its position.

- GPS – If the GPS signal is available and people are equipped by GPS units, then their position in a car can be determined. However, GPS suffers from lack of precision and its signal is not available everywhere (e.g. in tunnels).

- RFID – If each person wears a tag, then each person can be properly detected.

There are many publications on indoor localization:

- In [5.7], target objects are located by a wireless sensor network computing the Received Signal Strength Indicator.

- In [5.8], visible light communication is used to locate objects inside a building. Identification data is read from visible light tubes.

- In [5.9], thermal detection is used for indoor localization. Thermal sensors create a grid of 16 × 16 elements attached to the ceiling. The position of a person in the room is computed from responses of sensors.

In [5.10], UWB radio signals (different frequencies and bandwidths) are evaluated for localization because the presence of moving people modifies the indoor propagation channel. The authors in [5.11] evaluate and compare two localization techniques (Trilateration and Min-Max) using received signal strength and time of arrival techniques. Their study shows than the trilateral technique has better accuracy than the min-max one. A more accurate localization was achieved with the finger printing technique using on UWB standard [5.12]. The accuracy achieved was 0.5 meters. Study [5.13] proposes using the trilateration localization algorithm and applying the Unscented Kalman Filter algorithm to improve the accuracy (0.1 meters) of the localization. Finger printing cannot be used for small spaces due to random scattering energy in small spaces such as a car [5.1]. Because energy is distributed randomly in small spaces, we decided to use neural networks because it is easier than designing complex signal processing with uncertain results.

In [5.14] and [5.15], the authors used a Wi-Fi monitor to collect the data frame to determine the user's activity rather than obtaining their exact position. The research of Wi-Fi localization focusing [5.16] on this approach is based on the range using the equation to describe the relation between the observed signal and the location. On the basis of the observed signal to construct a map, and used deterministic techniques such as the K-nearest neighbor or the probabilistic methods such as Bayesian to estimate the device position. All the techniques mentioned in the previous text are used for indoor localization.

The research is aimed at estimating the number and the positions of people and as an example of localization of people, localization of passengers in a car was selected from CTF measured between the transmit antenna (TXA) and the receive one (RXA). The RXA antenna is situated inside the car at the front, and the TXA antenna is located inside the rear part of the car. The CTF is measured at UWB frequencies (3 GHz to 11 GHz). The measured channel transmission functions are evaluated by artificial neural networks (ANN). The CTF between antennas is the input of the ANN. Information about occupied seats is the output of the ANN.

The wave propagation in the car is influenced by reflections from the ceiling, windows, seats, luggage, etc.). Also, passengers in the car influence the CTF, and the influence is specific for each configuration of passengers. Properly processing the measured CTF can therefore reveal the number and the position of passengers in a car.

In order to estimate the occupied seats in a vehicle, transmissions between antennas in the car were measured. Configuration of the measurement setup is shown in Figure 5.28. The transmit antenna was successively placed to two positions. The first position was at the back left corner of the roof, and the second position was at the center of the roof. The receive antenna was successively located to three positions. The first position was in the front right corner, the second in the front center and the third one in the front center of the roof. Measurements were carried out in a Skoda Octavia III Sedan.

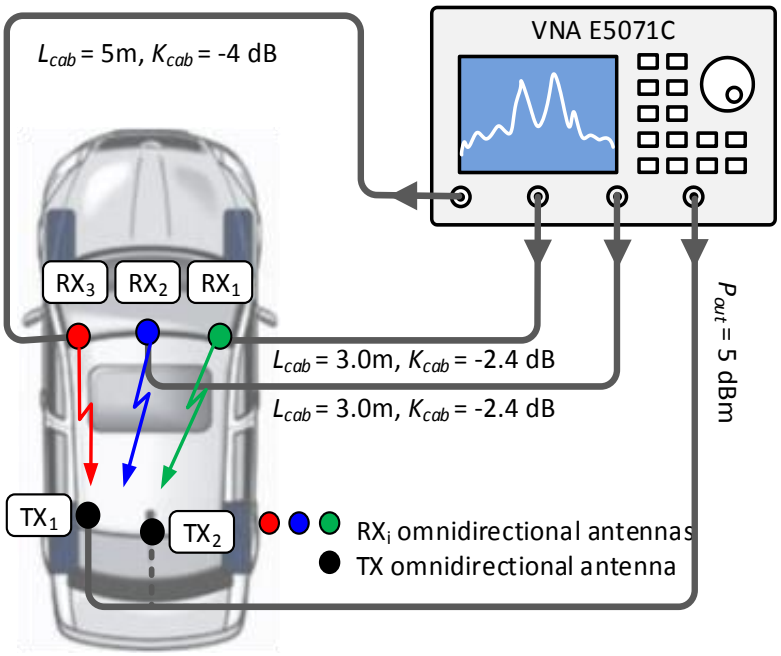

Figure 5.28: Schematics of measurement setup.

For each TXA–RXA configuration, the transmission between antennas S21 was measured by the four-port vector network analyzer (VNA) Agilent Technologies E5071C. The output power was set to 5 dBm. The resolution bandwidth used for measurements was 100 Hz due to the high dynamics of signals (110 dB, approximately).

Transmissions were measured from 3 GHz to 11 GHz with a frequency step of 10 MHz. For each configuration, transmission was measured at 801 frequencies. For measurements, we used mono-cone antennas connected to the VNA by phase stable coaxial cables published in [5.17]. Radiation patterns of the antenna are shown in Figure 5.29.

Measurement setup of transmissions between TXA antennas and RXA antennas is shown in Figure 5.30. Transmissions were measured for all possible combinations of people in the car. Each combination was measured five times to suppress random variations (e.g. movement of people in the car).

Outputs of measurements were used to train an ANN. The trained ANN was exploited to estimate occupied seats from measured transmissions in a different car occupied by different passengers sitting in slightly shifted positions (to demonstrate robustness of the trained neural estimator).

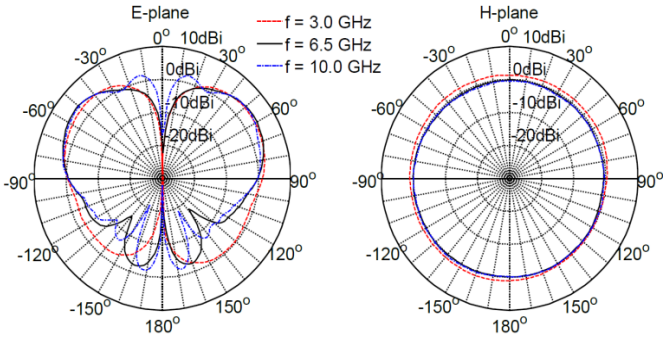

Figure 5.29: Radiation patterns of used mono-cone antennas [5.17].

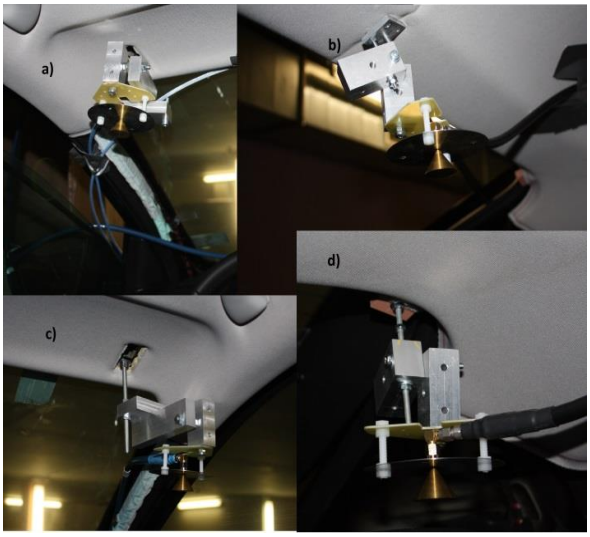

Figure 5.30: Monocone antennas for experimental characterization of channel transmission functions: a) receive antenna RXA3, b) transmit antenna TXA2, c) receive antenna RXA1, d) transmit antenna TXA1.

Figure 5.31 shows measured values of the transmission between the transmit antenna TXA1 and the receive antenna RXA1 (red points). In this configuration, the longest distance between antennas is achieved, and the transmitted wave covers the largest area in the car. The values were filtered to partially smoothen data (blue line); smoothing of the measured data is equivalent to a low-pass filtering [5.18]. The measured values were fitted by the FIR and the Matlab function fir1 was used with parameters: filter order 11 and frequency constrains 0.12 which ensures a good fit. Filtered signals were used for training neural networks. ANNs were implemented in the Neural Network Toolbox of the Matlab.

The FF ANN was trained by the Levenberg–Marquardt algorithm [5.19] which represents one of the most popular algorithms to train feed-forward neural networks and it is one of the methods that has been proven to be very efficient. The Levenberg - Marquardt algorithm uses an

approximation of the Hessian matrix [5.20] which requires only first order derivatives to be computed. This approximation, together with the trust region method [5.21] was used.

The Bayesian regularization algorithm [5.22] is not optimal because it easily converges to local minimum and not to the global optimum point (which is required). The Bayesian regularization algorithm is computationally more demanding than the Levenberg–Marquardt algorithm.

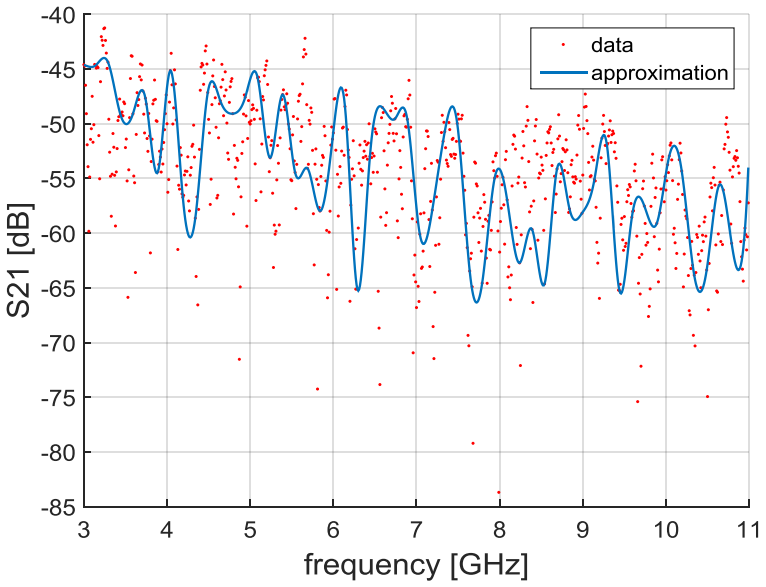

Figure 5.31: Measured frequency response of the transmission between the transmit antenna and the receive antenna (red). Polynomial approximation of frequency response of the transmission (blue).

For training the RBF ANN, each RBF neuron computes a measure of the similarity between the input and its prototype vector (taken from the training set). Input vectors which are more similar to the prototype return a result closer to 1. There are different possible choices of similarity functions, but the most popular is based on the Gaussian. Below is the equation for a Gaussian with a one-dimensional input [5.23]

$$f(x) = \frac{1}{\sigma\sqrt{2\pi}} e^{-\frac{(x-\mu)^2}{2\sigma^2}}$$

Here, x is the input, μ is the mean, and σ is the standard deviation.

In the training set:

- The input pattern was a vector consisting of magnitudes of the transmission between antennas S21 for a given combination of passengers. When composing the input pattern, each 15th value from the measured transmissions (3 GHz to 11 GHz) was selected; this corresponds to a 150 MHz frequency step and 53 samples.
- The output pattern was the corresponding combination of passengers.

All output targets (i.e., all combinations of passengers) are given in Table 5.1. The letter O indicates an occupied seat, and the letter N is associated with an unoccupied seat.

Table 5.1 Output targets of the training set. O: occupied seat, N: empty seat. White cell: correctly identified by RBF ANN, gray cell: incorrectly identified by RBF ANN.

pattern	*driver*	*seat 1*	*seat 2*	*seat 3*	*seat 4*
1	O	O	O	O	O
2	O	O	O	O	N
3	O	O	O	N	O
4	O	O	O	N	N
5	O	O	N	O	O
6	O	O	N	O	N
7	O	O	N	N	O
8	O	O	N	N	N
9	O	N	O	O	O
10	O	N	O	O	N
11	O	N	O	N	O
12	O	N	O	N	N
13	O	N	N	O	O
14	O	N	N	O	N
15	O	N	N	N	O
16	O	N	N	N	N
17	N	O	O	O	O
18	N	O	O	O	N
19	N	O	O	N	O
20	N	O	O	N	N
21	N	O	N	O	O
22	N	O	N	O	N
23	N	O	N	N	O
24	N	O	N	N	N
25	N	N	O	O	O
26	N	N	O	O	N
27	N	N	O	N	O
28	N	N	O	N	N
29	N	N	N	O	O
30	N	N	N	O	N
31	N	N	N	N	O
32	N	N	N	N	N

During training, the input patterns were introduced to the input of the ANN, and weights were changed to obtain corresponding output targets at the output of the ANN. The training process was stopped when the relative training error reached 10^{-6}, or the number of training cycles reached 100 for RBF ANN or 300 for FF ANN. Training was carried out in a Skoda Octavia III Sedan. For the same car, ANN was verified with other passengers.

Configuration of RBF ANN is identical with the structure depicted in Figure 5.3. Symbols x_1 to x_n denote input signals, w_{11} to w_{nm} are synoptic weights of neurons, and f_1 is an output signal.

In case of FF ANN, the Levenberg–Marquardt training algorithm and the Bayesian regularization training algorithm were applied. ANN contained three hidden layers with 15 neurons in the first layer, 20 neurons in the second layer and 5 neurons in the last layer. And all

the hidden neurons had the unipolar sigmoid activation function. Configuration of FF ANN used for the estimation of the passengers in the car is shown in Figure 5.32. Symbols x_1 to x_n denote input signals, w_{11} to w_{nm} are synoptic weights of neurons, and f_1 is an output signal.

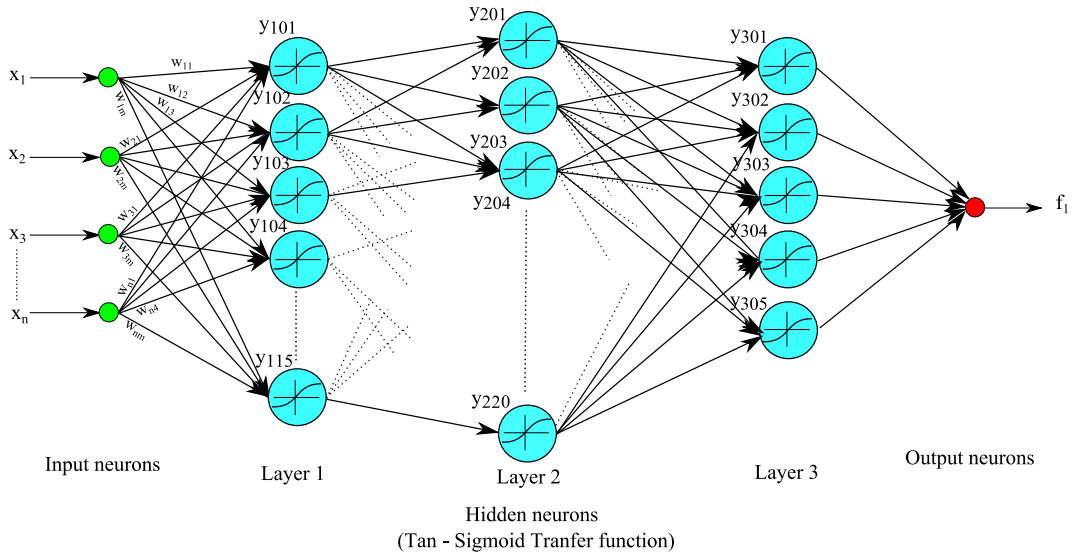

Figure 5.32: FF ANN used for estimating passengers in a car.

Training started with randomly set synoptic weights for all ANN. Training the RBF ANN took 90 seconds and training the FF ANN took 250 seconds with the Levenberg–Marquardt algorithm and 340 seconds with the Bayesian regularization algorithm.

The trained ANNs were used to estimate the configuration of passengers in the car. First, training patterns were used, but shifted frequency samples were introduced to the input of ANNs. In Figure 5.33, white cells indicate incorrect neural identification, and grey cells are associated with a correct neural estimation.

In order to verify the robustness of the trained ANN, testing patterns differing from training ones were used. Whereas training patterns consisted from each 15th frequency sample (3.00 GHz, 3.15 GHz, 3.30 GHz, …), testing samples were selected randomly between the 1st sample and the 14th one within each 15-sample subset of five independent measurements. For example (3.06 GHz, 3.21 GHz, 3.36 GHz, …), or (3.11 GHz, 3.26 GHz, 3.41 GHz, …).

The new testing samples were created according to of the previous description. The function was verified for all three types of ANN (RBF, FF with Bayesian regularization training algorithm and FF Levenberg–Marquardt training algorithm). The results of testing are show in the Figure 5.34.

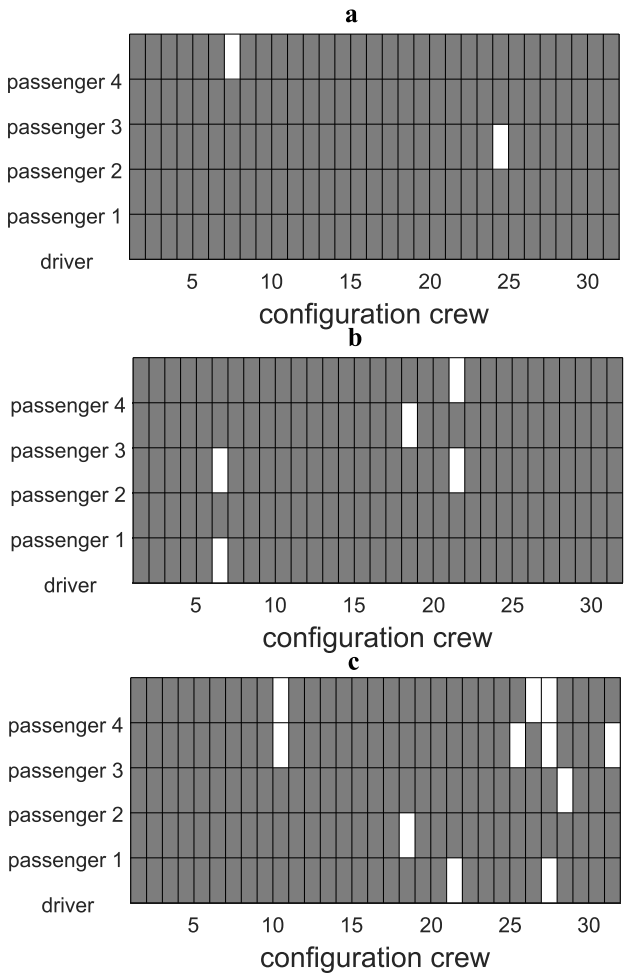

Figure 5.33: The number of wrong estimates for 32 standard configurations of passengers: a) RBF, b) FF Bayesian regularization, c) FF Levenberg–Marquardt algorithm.

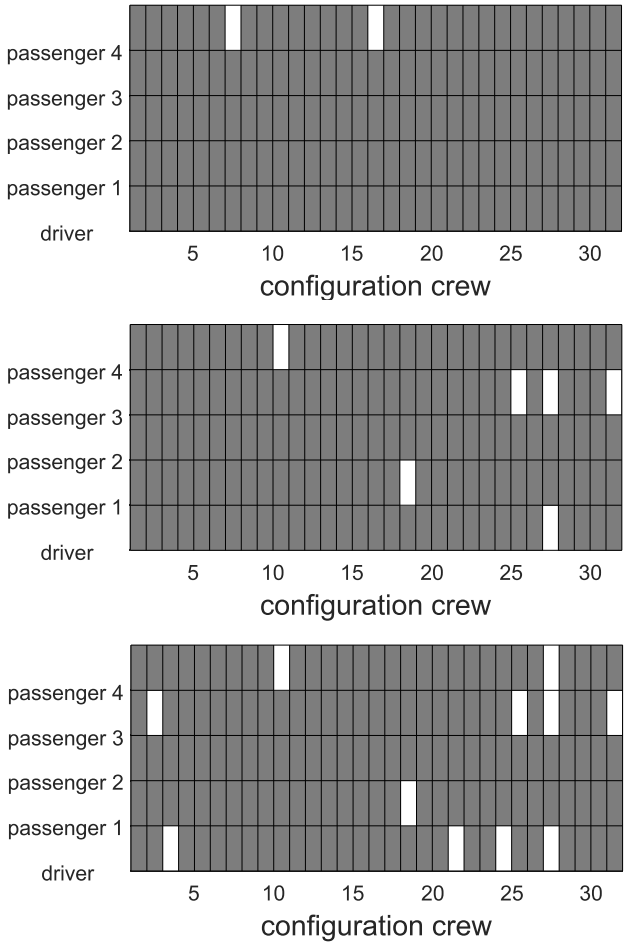

Figure 5.34: The number of wrong estimates for 32 standard configurations of passengers: a) RBF, b) FF Bayesian regularization, c) FF Levenberg–Marquardt algorithm.

The RBF ANN has the best accuracy from using ANN for localization of passengers. Another test sample was created for testing only the RBF ANN. The results of robustness testing of the RBF ANN are given in Figure 5.35.

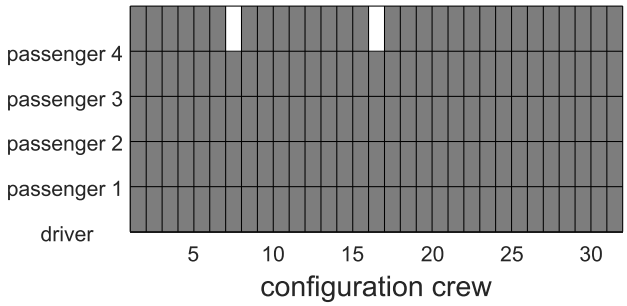

Figure 5.35: Verification of the number of wrong estimates for 32 standard configurations of passengers.

For patterns 7 and 17, ANN incorrectly estimates that the empty seat 4 is occupied in case of pattern 7 and incorrectly estimates that the empty seat 4 is occupied in case pattern 17. The examples verify estimated the RBF ANN for correct pattern 3 and incorrect pattern 7 (see Figure 5.36).

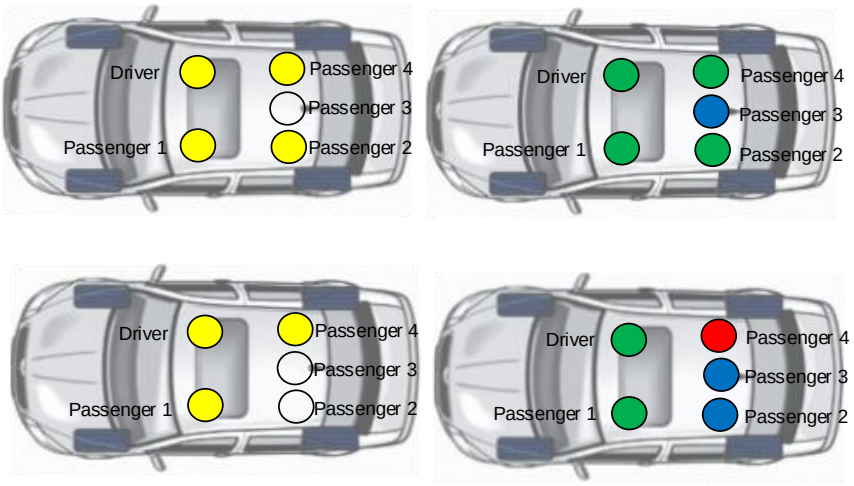

Figure 5.36: Combinations of passengers identified by RBF ANN.
Top: pattern 3, bottom: pattern 7. Yellow: occupied seat,
green: correctly identified seat, red: incorrectly identified seat.

Previous research was aimed to use the whole UWB frequency bandwidth, which is an disadvantage. The whole UWB frequency bandwidth is occupied when detecting the position and number of passengers in the car. The frequency bandwidth from 6.0 GHz to 7.4 GHz was selected for eliminating this disadvantage.

All the above mentioned procedures were applied on the bandwidth 6.0 GHz to 7.4 GHz and the neural networks were created and trained with the same parameters. The results are shown in Figures 5.37 and 5.38.

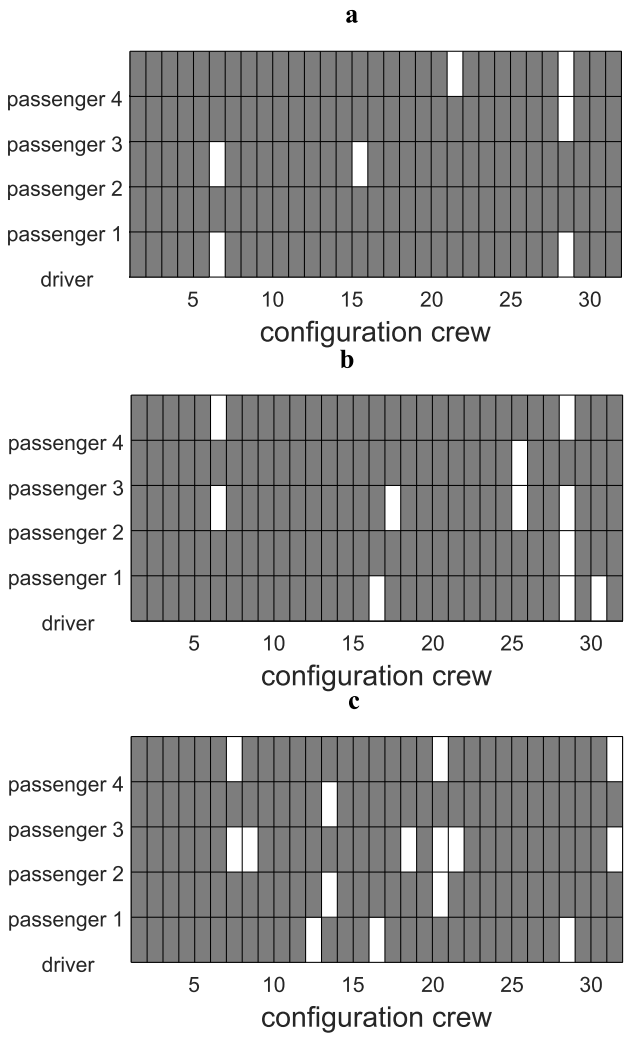

Figure 5.37: The number of wrong estimates for 32 standard configurations of passengers for frequency bandwidth 6.0 GHz to 7,4 GHz: a) RBF, b) FF Bayesian regularization, c) FF Levenberg–Marquardt algorithm.

Figures 5.37 and 5.38 can show than the accuracy of passenger localization decreases while maintaining the same conditions and parameters of training. This is caused by the lower quantity of training samples compared to the whole UWB band. The FF ANN with the Levenberg-Marquardt training algorithm has the lowest accuracy from all the NN used. The FF ANN with the Bayesian regularization is more accurate, and the RBF ANN is the most accurate. This result corresponds with previous outputs.

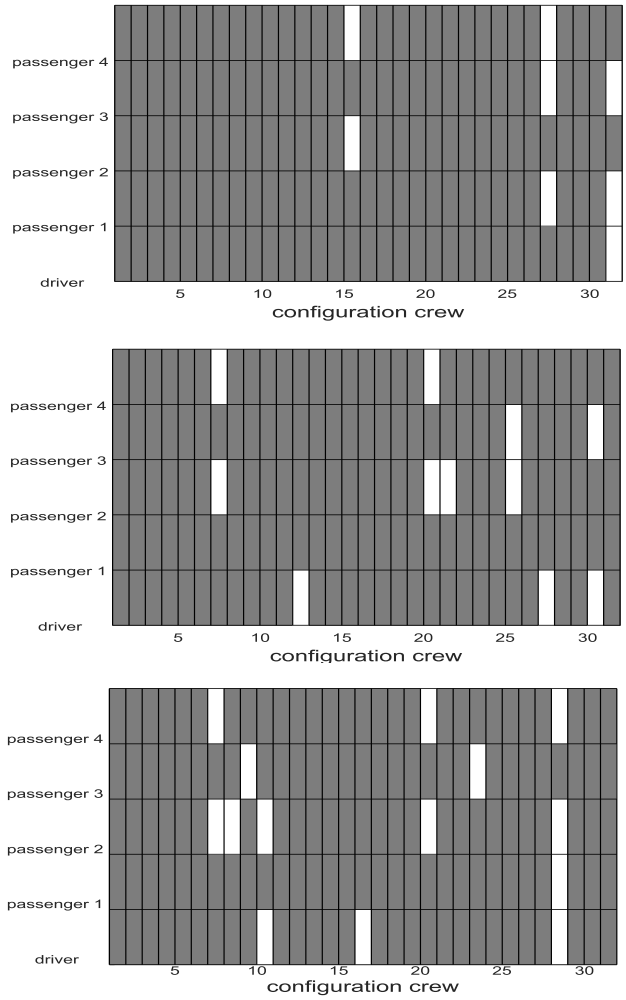

Figure 5.38: The number of wrong estimates for 32 standard configurations of passengers for frequency bandwidth 6.0 to 7.4 GHz: a) RBF, b) FF Bayesian regularization, c) FF Levenberg–Marquardt algorithm.

The training and verification patterns were created from measured frequency responses of the transmission between antennas. The radial basis function (RBF) ANN and feed-forward (FF) ones showed different estimation abilities:

- Estimations provided by FF ANN were inaccurate due to extensive dynamics of the CTF in the car. Hence, FF ANNs are not suitable for identifying passengers. The percentage of success for passenger position estimation using trained FF ANN and the entire UWB with the Levenberg–Marquardt algorithm is 93.12%, and using the Bayesian regularization is 96.34%. For the case of the 6.0 to 7.4 GHz band the results of estimation are 89.45% using the Levenberg–Marquardt algorithm and 93.12% using the Bayesian regularization.

- Estimations provided by the RBF ANN in the entire UWB bandwidth were relatively accurate with a success percentage of 98.75% (only configurations 8 and 24 were estimated incorrectly). For the case of the 6.0 to 7.4 GHz band, the success rate is 95.75% for person position estimation.

Table 5.2 compares achieved localization results inside the car with using the ANN:

- The first half of Table 5.2 shows the results achieved for the UWB band 3.0 to 11 GHz. The most important parameter is the achieved accuracy (reliability) of the localization which reaches 98.75%.
- The second half of Table 5.2 shows the results for the UWB band 6.0 to 7.4 GHz. For this bandwidth, the accuracy of localization is 95.75%. The lower value is due to the lower number of training samples.

Another important parameter is the training time. The UWB band 6.0 to 7.4 GHz needs half of the training time compared to the UWB band 3 to 11 GHz. The training time is shorter because we use a lower number of training samples.

Table 5.2 Comparison of basic ANN parameters and achieved accuracy.

	Neural network	Number samples CTF	Training time [s]	Number training cycle	Accuracy
UWB 3-11 GHz	RBF	53	90	100	98,75
	FF - LM	53	250	300	96,34
	FF - RB	53	340	300	93,12
UWB 6-7.4 GHz	RBF	10	45	100	95,75
	FF - LM	10	130	300	93,12
	FF - RB	10	175	300	89,45

The number of wrong estimates and position of passengers is shown in Figure 5.39. The number of mistakes increases because the number of training samples of the ANN is much smaller. The accuracy of localization is rapidly decreasing, reaching the number of training patterns 10. These results were expected.

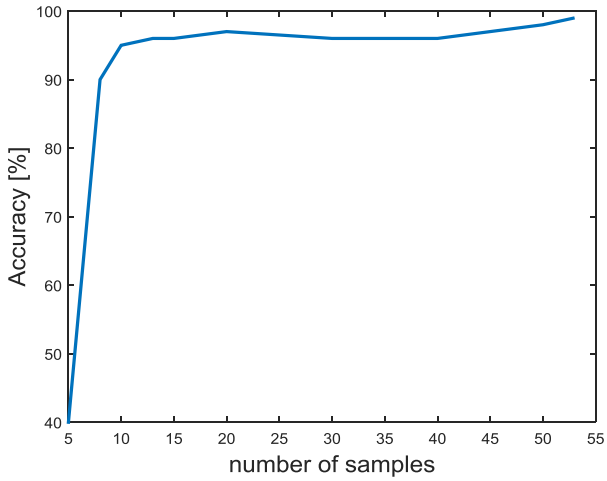

Figure 5.39: The estimated accuracy (ANN RBF) depending on the number of training samples.

Previous results have shown that location accuracy is relatively reliable and accurate. However, localization errors occur, especially in the case of a lower number of training samples. Increasing the accuracy of localization could be achieved by optimizing antenna deployment. Another way how to increase accuracy comprises of averaging a few position estimations. The accuracy would be increased by optimizing the ANN and their parameters.

5.5 Conclusions

Methodology of the approximation of outputs of in-car measurements by artificial neural networks is worked out suitable neural approximation with optimally architecture of the networks. The radial basis function and feed-forward neural networks were selected as the most appropriate.The next step was to explore the most suitable neural architecture to create training sets of measured values.

- The wireless power transfer along an inner surface of a vehicle on the 60 GHz ISM band. The models channel transfer functions were created using RBF and FF neural models. Created model was verified. The estimation error of the channel transfer function between the transmit antenna and the receive antenna does not exceed the level of 4 per cent. These models can be used to predict the shape of the channel transfer function.

- To verify the creation the small wireless networks for the distribution of data services such as internet, video, audio, etc. The neural models of the UWB frequency band estimation from 3 GHz to 11 GHz are created. The neural models are created using measured values in the car. Various neural networks (RBF and FF network) are used to create neural models to better compare results. Estimation errors are approximately 4 percent. The accuracy of the channel transfer function is sufficient.

- A neural estimator of seats occupied by passengers in a vehicle is introduced in the next chapter. The estimator is built from the RBF neural architecture. The seat occupied is obtained from channel transfer function between antennas operating in 60 GHz ISM band. The results show that the estimator reaches a maximum of 1 error per crew configuration in the car. Improved accuracy of the estimate can be achieved by additional data processing.

- For this case of localization passengers in the car was selected bandwidth from 3 to 11 GHz. For localization, two types of neural architectures are used the FF and the RBF. The channel transfer function was measured at ultra-wideband frequencies (3 to 11 GHz) which used for trained neural networks. The monocone antennas were used for measurement. The accuracy of the estimate is achieved for RBF is 98.75% and for the FF neural architecture is 93.12%. Therefore it is more suitable for locating passengers RBF neural architecture.

It can be concluded from the above that selected neural architectures and data processing can be used to estimate channel transfer function and localization passengers in the car.

5.6 References

[5.1] J. Blumenstein, T. Mikulasek, R. Marsalek, A. Prokes, T. Zemen and C. Mecklenbräuker, In-vehicle mm-wave channel model and measurement, *Vehicular Technology Conference* (VTC Fall 2014), Vancouver, Canada, 2014.

[5.2] J. Ren, C. Cai, H. Zhao and Z. Xie, Research and simulation analysis of UWB indoor channel model, *International Conference on Computer Science & Service System* (CSSS 2012), Nanjing, China, p. 1228-1231.

[5.3] W. Niu, J. Li and T. Talty, Intra-vehicle UWB channels in moving and stationary scenarios, *Military Communications Conference* (MILCOM 2009), Boston, USA, 2009.

[5.4] M. Schack, J. Jemai, R. Piesiewicz, R. Geise, I. Schmidt and T. Kurner, Measurements and analysis of an in-car UWB channel, *Vehicular Technology Conference* (VTC Spring 2008), Singapore, 2008, p. 459-463.

[5.5] A. Chandra; A. Prokes; T. Mikulasek; J. Blumenstein; P. Kukolev; T. Zemen; C. F. Mecklenbrauker, Frequency-domain in-vehicle UWB channel modeling, *IEEE Transactions on Vehicular Technology*, 2016, vol. 65, no. 6, p. 3929-3940.

[5.6] T. Sanpechuda and L. Kovavisaruch, A review of RFID localization: applications and techniques, *5th International Conference on Electrical Engineering / Electronics, Computer, Telecommunications and Information Technology* (ECTI-CON 2008), Krabi, Thailand, 2008, p. 769-772.

[5.7] A. Guidara and F. Derbel, A real-time indoor localization platform based on wireless sensor networks, *12th International Multi-Conference on Systems, Signals and Devices*, 2015.

[5.8] P. Cherntanomwong and W. Chantharasena, Indoor localization system using visible light communication. 7th International Conference on Information Technology and Electrical Engineering, 2015, p. 480-483.

[5.9] M. Kuki, H. Nakajima, N. Tsuchiya and Y. Hata, Multi-human locating in real environment by thermal sensor, *IEEE International Conference on Systems, Man, and Cybernetics*, 2013, p. 4623-4628.

[5.10] C. Laderriere, M. Heddebaut, J. Prost, A. Rivenq, F. Elbahhar and J. M. Rouvaen, Wide-band indoor localization effectiveness in presence of moving people, *Positioning, Navigation and Communication*, 2008, p. 103-111.

[5.11] S. Promwong and P. Southisombat, UWB transmission measurement and modeling for indoor localization, International Computer Science and Engineering Conference (ICSEC 2016), Chiang Mai, 2016.

[5.12] W. Vinicchayakul, S. Promwong and P. Supanakoon, Study of UWB indoor localization using fingerprinting technique with different number of antennas,

International Computer Science and Engineering Conference (ICSEC 2016), Chiang Mai.

[5.13] H. Yin, W. Xia, Y. Zhang and L. Shen, UWB-based indoor high precision localization system with robust unscented Kalman filter, *IEEE International Conference on Communication Systems* (ICCS 2016), Shenzhen.

[5.14] W. Yan, C. Yingying, and R. P. Martin, Leveraging Wi-Fi signals to monitor human queues, *IEEE Pervasive Computing*, 2014, vol. 13, no. 2, p. 14–17.

[5.15] J. Manweiler, N. Santhapuri, R. R. Choudhury, and S. Nelakuditi, Predicting length of stay at WiFi hotspots, *IEEE INFOCOM*, Turin, Italy, 2013, p. 3102–3110..

[5.16] H. Chen, Y. Zhang, W. Li and P. Zhang, Non-cooperative Wi-Fi localization via monitoring probe request frames, *Vehicular Technology Conference* (VTC-Fall 2016), Montreal, Canada, 2016.

[5.17] T. Mikulasek, J. Blumenstein and A. Prokes, Antennas utilized for intra-vehicle 3-11 GHz and 55-65 GHz channel measurement, PIERS, 2016.

[5.18] D. F. Specht, A general regression neural network, *IEEE Transactions on Neural Networks*, 1991, vol. 2, no. 6, p. 568-576.

[5.19] H. P. Gavin, *The Levenberg-Marquardt method for nonlinear least squares curve-fitting problems*, Department of Civil and Environmental Engineering, Duke University, 2016.

[5.20] A. K. Jain, M. Jianchang; K. M. Mohiuddin, Artificial neural networks: a tutorial, *Computer*, 1996, vol. 29, no. 3, p. 31-44.

[5.21] N. M. Drawil, H. M. Amar and O. A. Basir, GPS localization accuracy classification: a context-based approach, *IEEE Transactions on Intelligent Transportation Systems*, 2013, vol. 14, no. 1, p. 262-273.

[5.22] Jingwen Tian; Meijuan Gao; Fan Zhang, Network intrusion detection method based on radial basic function neural network, *International Conference on E-Business and Information System Security* (EBISS 2009), 2009.

[5.23] M. Kotol, Z. Raida, J. Láčík, Neural-Network Based In- Vehicle Localization Passengers. In International Conference, *Radioelektronika 2016*. IEEE Xplore, 2016. s. 100-104. ISBN: 978-1-5090-1673- 0.

[5.24] M. Kotol, Z. Raida, Comparison of Neural Models of UWB and 60GHz, In- car Transmission Channels. *CoBCom 2016*. IEEE Xplore, 2016. s. 64-68. ISBN: 978-1-5090-2269- 4.

[5.25] M. Kotol, The Neural models for differrent training algorithms. *Student conference Blansko 2016*. http://www.ieee.cz/: 2016. s. 31-34. ISBN: 978-80-214-5389- 0.

[5.26] M. Kotol, A. Prokeš, T. Mikulášek, Z. Raida, Estimation The Transmission Between Antennas Using Artificial Neural Networks In The Uwb Band. *Progress in Electromagnetic Research Symposium (PIERS) 2016*. IEEE Xplore, 2016. s. 1465-1469. ISBN: 978-1-5090-6093- 1.

[5.27] M. Kotol, Z. Raida, Neural Model Of Transmission Channel, In 60 Ghz Ism Band. *Student EEICT. 2016*. s. 328-332. ISBN: 978-80-214-5350- 0.

[5.28] J. Vélim, Z. Raida, J. Láčík, J. Lambor, M. Kotol, On- roof wireless link operating at 60 GHz. *IEEE-APS Topical Conference on Antennas and Propagation in Wireless Communications (APWC). 2015*. s. 153-156. ISBN: 978-1-4799-7808- 3.

[5.29] M. Kotol, J. Vélim, Z. Raida, Neural Modeling Of In-Vehicle Wireless Channels: Wave Propagation Along The Vehicle Body at 60 GHz. In 2015 *IEEE-APS Topical Conference on Antennas and Propagation in Wireless Comunications (APWC). 2015.* s. 279-282. ISBN: 978-1-4799-7808- 3.

[5.30] M. Kotol, Estimation Of Statistical Parameters Of The Digital Signal Using Artificial Neural Networks. *Student conference Kohútka 2015.* http://www.ieee.cz/:.s. 21-24. ISBN: 978-80-214-5239- 8.

Chapter 6

Conclusions

The focal point of the dissertation consists in modeling the electromagnetic field and the CTF in the interior of the car. For modeling are used ANN that may be more effective than traditional methods analysis.

A look at the history of ANN shows that the first theoretical model of artificial neuron originated was created in the mid-twentieth century. The perceptron and first mathematical models (perceptron network, multilayer perceptron network) followed. Another development was to create Hopfield's NN, FF ANN, RBF ANN, etc.

The state of the art NN general and their function briefly summarized in the beginning section. The ANN can be used for solution of wide range of issues. The ANN can be also used for the solution of electromagnetic compatibility (EMC) problems [2.15]. For estimating the channels of the downlink of the LTE system, ANN has been used too [2.19]. The ANN estimated a suitable channel for downlink from the parameters of OFDM pilot channels. It is shown that modeling wireless channels by ANN is possible for a indoor and outdoor communication channel and a properties this communication channel.

The next step was to explore the possibilities of spreading EM waves inside the car. Because, the modern automobiles contain a multitude of wireless transmission systems, e.g., for mobile, in car communication and car-to-x communications for connect the acquisition of information with the operational status of cars. The research is aimed on two directions from the perspective of frequencies. The first direction explores the frequency range 55-65 GHz, the ideal location of the antennas, the frequency range, the appropriate communication technology [2.37], [2.38], [2.39]. The second direction is aim on the 3 to 11 GHz frequency band and tries to use the existing technology to create a communication channel inside the car or the car to car [2.40], [2.41], [2.42], [2.43].

This work is divided into two main objectives.

Objective 1

Methodology of experimental characterization of wireless channels in vehicles will be worked out with the emphasis on the exploitation of measured data for the training of artificial neural networks. The CTF in the interior of a car will be experimentally characterized in frequency ranges from 55 GHz to 65 GHz and from 3 GHz to 11GHz. Validity of selected measurements will be verified by simulations in proper software and approximate analytical models.

The work presented within this treatise deals with the design of EM wave propagation mechanisms were investigated inside the car. On the wave propagation is involved three basis mechanism propagation (surface wave, direct wave and reflected wave), of which the largest share of energy propagation has a surface wave. Based on previous findings, numerical models

for the 2.4 GHz, 5.8 GHz and 60GHz have been developed that are validated by measurement in laboratory conditions and in real-world vehicle conditions for the 2.4 GHz and 5.8 GHz frequencies using monopole antennas and waveguides. The results of numerical models and measurements show that 2.4 GHz is best suited for the distribution of wireless services in the interior of the car and the use of a waveguide as the transmitting antenna. Measurement at 60 GHz in this work is not available because suitable measuring antennas are not available.

Objective 2

Methodology of the approximation of outputs of in-car measurements by artificial neural networks will be worked out. Neural approximations will be investigated from the viewpoint of an optimally architecture of the network, convergence of the training process, an optimal composition of training sets and a proper validation. Neural models will be developed for various in-car applications (statistical characterization of channel transfer functions, identification of objects in a car, etc.).

The methodology of the approximation of outputs of in car measurements is based on the filtering of measured values and the reduction of input data dynamics, with an emphasis on grasping the shape of the transmission function. Because the high input data dynamics is not suitable for NN. The NN architecture to modeling the CTF are selected by FF and RBF type. New data were used to verify the function of trained neural networks. Neural models have developed applications that are described below.

From the point of view of frequency, application part of this work is directed in two directions. The first direction is for the 60 GHz frequency band. These frequencies will be used in the near future for service distributions and the creation of local networks within the car. The second direction focuses on 3 - 11 GHz (UWB) frequencies. In this frequency band, it is possible to use existing technology to create local networks inside the car. Nowadays, numerical modeling at high frequencies is very time-consuming and computationally challenging. That's why I focused on modeling and estimating CTF using ANN.

In the next part of my work I focused on estimating the CTF using ANN in the 60 GHz band and 3 - 11 GHz (UWB) frequencies. For these, measurements were made of the CTF in the interior of the car between the transmitting and receiving antenna. The measured values were used to train and verify the ANN. To estimate the CTF, two ANN (FF, RBF) tips were used to better compare the results.Functionality of neural models was verified on testing patterns which differ from training ones by the frequency. The results show that the estimation error does not exceed the level of 4 per cent for both used the ANN in the case 60 GHz band. For the 3 - 11 GHz band, the estimation error is approximately the same as the 60 GHz band. From the results we can conclude that for a quick estimate the CTF we can use artificial neural networks.

Using the knowledge of previous research, I found out that the passengers in the car have a great influence on the shape of the CTF. Therefore the last part of the work is devoted to the practical application of the ANN to locate the passengers inside the car. From the frequency point of view, I focused on two directions in the frequency range 55-65 GHz and 3 - 11 GHz. For the optimal achievable accuracy of localization was the implementation of practical measurements in the car. When Tx and Rx were in a firm place, it was measured how the

passengers inside the car had an influence on the CTF. This measurement was realized for different passengers in order to achieve greater objectivity. The measured values were used to train and verify the ANN to locate the passengers in the car. Two different ANNs were used again for better comparison. The results show that the RBF ANN is more suitable for locating the position of passengers inside the car, which achieves about half the better accuracy.